Copy No._____

Defence Research and Development Canada
Recherche et développement pour la défense Canada

DEFENCE R&D DÉFENSE

Hydrodynamic Forces and Motions in the Time Domain for an Unappended Ship Hull

Kevin McTaggart

Defence R&D Canada

Technical Memorandum
DRDC Atlantic TM 2003-104
May 2003

Canada

This page intentionally left blank.

Hydrodynamic Forces and Motions in the Time Domain for an Unappended Ship Hull

Kevin McTaggart

Defence R&D Canada – Atlantic

Technical Memorandum

DRDC Atlantic TM 2003-104

May 2003

Author

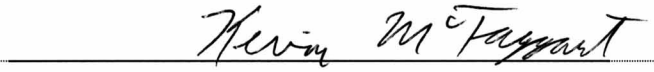

Kevin A. McTaggart

Approved by

Neil Pegg

Head, Warship Performance

Approved for release by

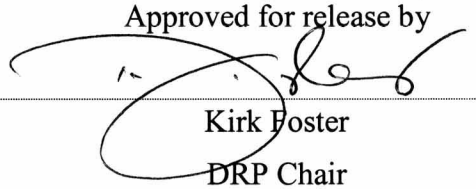

Kirk Foster

DRP Chair

Abstract

This report describes numerical predictions of hydrodynamic forces and motions in the time domain for an unappended ship hull in waves. The hydrodynamic forces in the time domain are evaluated using previously computed values in the frequency domain, which are based on the three-dimensional Green function for a body with zero forward speed. Forward speed effects are included in both the frequency and time domains using suitable approximations. Due to the underlying importance of numerical predictions of hydrodynamic forces in the frequency domain, attention has been given to their accuracy, robustness, and efficiency. Comparisons between motion predictions in the frequency and time domains show excellent agreement, suggesting correct theoretical and numerical implementations. Comparisons of numerical heave and pitch predictions with model test data for the frigate HALIFAX show very good agreement. Time domain simulations of ship motion execute significantly faster than real time, indicating that the approach will be practical for modelling and simulation applications.

Résumé

Dans ce rapport nous décrivons les prédictions numériques calculées dans le domaine temporel des forces hydrodynamiques et des mouvements d'une coque sans appendices dans les vagues. Nous avons évalué les forces hydrodynamiques dans le domaine temporel en utilisant les valeurs calculées antérieurement dans le domaine fréquentiel avec une fonction de Green tridimensionnelle pour un corps de vitesse avant nulle. Les effets de la vitesse avant ont été ajoutés dans les domaines fréquentiel et temporel en utilisant des approximations adaptées. Étant donné l'importance intrinsèque des prédictions numériques des forces hydrodynamiques dans le domaine fréquentiel, nous avons apporté une attention particulière à la précision, à la robustesse et à l'efficacité des calculs. L'accord entre les prédictions des mouvements dans les domaines temporel et fréquentiel est bon, ce qui suggère que la théorie et son implémentation logicielle soient correctes. L'accord entre les prédictions numériques du soulèvement et du tangage pour la frégate HALIFAX avec les données sur maquette est très bon. Le calcul des simulations des mouvements du navire dans le domaine temporel est beaucoup plus rapide que le calcul en temps réel, ce qui indique que l'on pourra utiliser notre méthode pour la modélisation et les simulations.

This page intentionally left blank.

Executive summary

Introduction

DRDC Atlantic is developing a new object-oriented library for simulation of ship motions in waves. A previous report presented predictions of ship hydrodynamic forces and motions in the frequency domain using a panel method. This report presents a method for extending hydrodynamic force and motion predictions to the time domain using previously computed values for the frequency domain.

Principal Results

Improvements have been made to accuracy, robustness, and computational speed of hydrodynamic force predictions in the frequency domain. New hydrodynamic force predictions in the time domain produce motions which are in agreement with predictions in the frequency domain, suggesting correct theoretical and numerical implementations. Comparisons of heave and pitch predictions with experimental results show very good agreement.

Significance of Results

New object-oriented software is now available for simulating motions in waves of an unappended ship. The new software uses a panel method, ensuring fidelity for non-slender hull forms such as the Canadian Navy's KINGSTON class. The inclusion of nonlinear forces from buoyancy and incident waves can contribute to accuracy of ship motion predictions in higher sea states. Both linear and nonlinear predictions run significantly faster than real time, which is important for simulation applications.

Future Plans

In the near term, forces from rudders, bilge keels, and other appendages will be incorporated into numerical predictions of ship motions in waves. In the longer term, the motions of a freely maneuvering ship in waves will be predicted.

Kevin McTaggart; 2003; Hydrodynamic Forces and Motions in the Time Domain for an Unappended Ship Hull; DRDC Atlantic TM 2003-104; Defence R&D Canada – Atlantic.

Sommaire

Introduction

RDDC assemble une nouvelle bibliothèque de logiciels orientés objet qui seront utilisés pour simuler le mouvement des navires dans les vagues. Dans un rapport précédent, nous avons présenté les prédictions des forces hydrodynamiques exercées sur le navire et de ses mouvements, calculées dans le domaine des fréquences avec la méthode des panneaux. Dans ce rapport, nous présentons une méthode permettant d'étendre les prédictions des forces hydrodynamiques et des mouvements, au domaine temporel, à partir des valeurs déjà calculées dans le domaine fréquentiel.

Résultats principaux

Nous avons amélioré la précision, la robustesse et la vitesse du calcul des prédictions des forces hydrodynamiques dans le domaine des fréquences. Les nouvelles prédictions pour la force dans le domaine temporel se traduisent par des mouvements qui concordent avec les prédictions dans le domaine fréquentiel, ce qui suggère que la théorie et son implémentation logicielle sont correctes. L'accord entre les prédictions pour le soulèvement et le tangage et les résultats expérimentaux est bon.

Importance des résultats

Un nouveau logiciel orienté objet permettant de simuler les mouvements d'un navire muni d'aucun appendice dans des vagues est maintenant disponible. Les prédictions de ce nouveau logiciel sont effectuées à partir de la méthode des panneaux, ce qui garantit l'exactitude des calculs pour les coques larges comme celles des navires de la classe Kingston de la Marine canadienne. L'ajout des forces non linéaires de la flottabilité et des vagues incidentes pourra contribuer à la précision des prédictions des mouvements des navires dans les mers très agitées. Le calcul linéaire et non linéaire des prédictions est beaucoup plus rapide que le calcul en temps réel, un élément important pour les simulations.

Travaux ultérieurs prévus

Nous incorporerons prochainement les forces exercées par les gouvernails, les quilles de roulis et autres appendices aux prédictions numériques des mouvements des navires dans les vagues. À plus long terme, on pourra prédire des mouvements de navires manœuvrant librement dans les vagues.

Kevin McTaggart; 2003; Hydrodynamic Forces and Motions in the Time Domain for an Unappended Ship Hull; DRDC Atlantic TM 2003-104; Defence R&D Canada – Atlantic.

Table of contents

List of tables

List of figures

1 Introduction

Simulations of ship motions in waves are required for numerous naval applications. When evaluating performance of crew and ship systems, the influence of ship motions is often significant. The safety of a ship will be highly dependent on its ability to resist capsize and wave-induced structural loads.

To facilitate simulation efforts, DRDC Atlantic is developing a new object-oriented library for predicting ship motions in waves. During development of this library, attention is being given to balancing requirements for fidelity, efficiency, and robustness. It was decided that these requirements could be satisfied by computing ship motions in the time domain using hull hydrodynamic forces derived from computations in the frequency domain. Reference 1 describes computation of hull hydrodynamic forces in the frequency domain using a panel method. The present report describes the evaluation of hydrodynamic forces in the time domain using previously computed results in the frequency domain. Section 2 gives a review of hydrodynamic coefficients in the frequency domain based on Reference 1. The theory for obtaining time domain forces from frequency domain values is presented in Section 3. Section 4 gives particulars for the ship HALIFAX, which is used for sample computations throughout the remainder of the report. Improvements to frequency domain computations are given in Section 5, followed by sample frequency domain coefficients in Section 6. Section 7 gives sample time domain coefficients based upon previously computed frequency domain values. Section 8 discusses computation of ship motions in the time domain using time domain hydrodynamic coefficients. To verify the new time domain approach, Section 9 compares motions computed in the time and frequency domains. The extension of time domain predictions to include nonlinear contributions from buoyancy and incident waves is described in Section 10, followed by validation of computations using experimental data in Section 11. Section 12 gives concluding remarks.

2 Review of Hydrodynamic Coefficients in the Frequency Domain

As mentioned previously, this report describes prediction of hull hydrodynamic forces in the time domain using previously computed frequency domain values. For completeness, a review of frequency domain coefficients from Reference 1 is presented here.

Figure 1 shows the coordinate system used for ship motion computations. The ship is assumed to move at steady forward speed and heading, and the coordinate system is a translating earth system moving with the steady forward speed. The origin of the translating earth system is located at the ship centre of gravity when the ship is in calm water. The location of the translating earth system is not affected by wave-induced ship motions. Note that the present coordinate system is slightly different from that used for solution of hydrodynamic forces in Reference 1, for which the vertical z axis passed through the centre of gravity but had its origin at the calm water surface. Reference 1 used a different origin because many computational terms were dependent upon elevation relative to the calm water surface. In the present axis system, elevation relative to the calm water surface is given by:

$$z_{wl} \;=\; z \;+\; \tilde{z}_{wl}^{CG} \tag{1}$$

where $\tilde{z}_{wl}^{CG}$ is the elevation of the ship centre of gravity relative to the calm water surface when the ship is at rest. Figure 2 gives the sea direction convention, with a heading β of 180 degrees representing head seas.

Oscillatory ship motions in the time domain are related to ship motions in the frequency domain as follows:

$$\eta_j(t) \;=\; \text{Real}\left\{\eta_j \;\exp(i\,\omega_e\,t)\right\} \;\text{for}\; j = 1-6 \tag{2}$$

where ω_e is wave encounter frequency given by:

$$\omega_e \;=\; |\omega_I \;-\; k_I\,U\;\cos\beta| \tag{3}$$

where ω_I is incident wave frequency, k_I is incident wavenumber, U is forward ship speed, and β is incident wave direction. Water depth is assumed to be large (i.e., greater than half the incident wavelength), and the following dispersion relation applies:

$$k_I \;=\; \frac{\omega_I^2}{g} \tag{4}$$

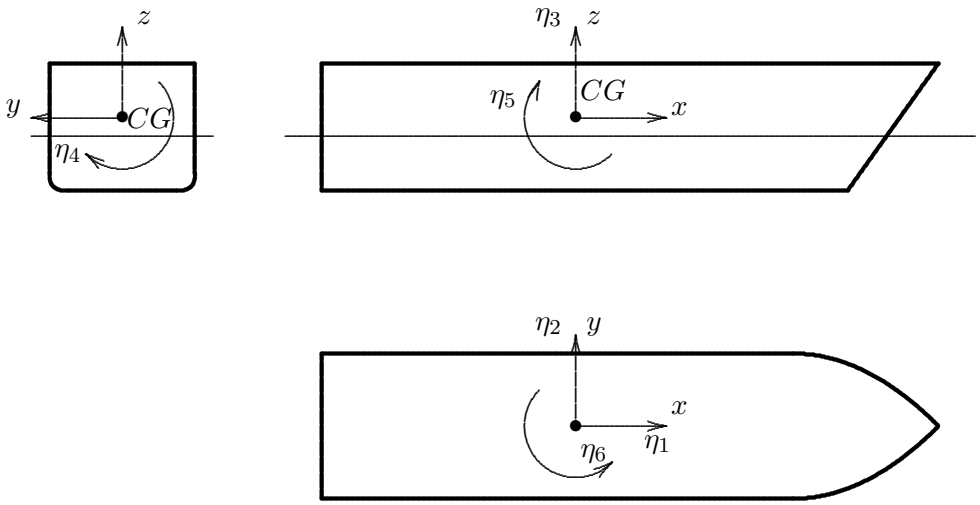

Figure 1: *Coordinate System for Solution of Hydrodynamic Forces*

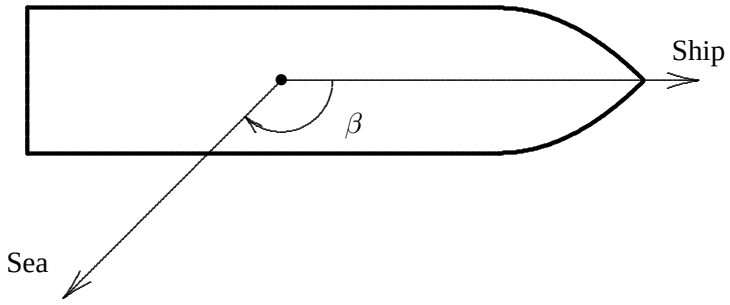

Figure 2: *Sea Direction for Solution of Hydrodynamic Forces*

where g is gravitational acceleration. The equations of ship motions in the frequency domain are given by:

$$\left\{-\omega_e^2\left([M]+[A]\right) \; + \; i\omega_e[B] \; +[C]\right\} \; \{\eta\} \;\; = \;\; \left\{F^I \; + \; F^D\right\} \tag{5}$$

where $[M]$ is the ship mass matrix, $[A]$ is the added mass matrix, $[B]$ is the damping matrix, $[C]$ is the stiffness matrix, $\left\{F^I\right\}$ is the incident wave excitation vector, and $\left\{F^D\right\}$ is the diffracted wave excitation vector. The added mass and damping matrix terms are given by:

$$A_{jk} \;\; = \;\; -\frac{\rho}{\omega_e}\int_{S_b}\left[\text{Imag}(\phi_k) \; + \; \frac{U}{\omega_e}\,\text{Real}\left(\frac{\partial\phi_k}{\partial x}\right)\right] n_j \; dS \tag{6}$$

$$B_{jk} \;\; = \;\; -\rho\int_{S_b}\left[\text{Real}(\phi_k) \; - \; \frac{U}{\omega_e}\,\text{Imag}\left(\frac{\partial\phi_k}{\partial x}\right)\right] \; n_j \; dS \tag{7}$$

where ρ is water density, S_b denotes the wetted surface of the ship, ϕ_k is the complex velocity potential due to oscillatory motions for mode k, and n_j is the outward normal component for mode j. Note that Equation (6) has a correction to a sign error for the speed term in Reference 1. The above equations can be rewritten to show speed dependent terms as follows:

$$A_{jk} \;\; = \;\; -\frac{\rho}{\omega_e}\int_{S_b}\text{Imag}(\phi_k)n_j \; dS \; - \; \frac{\rho}{\omega_e}\,\frac{U}{\omega_e} \; \int_{S_b}\text{Real}\left(\frac{\partial\phi_k}{\partial x}\right) n_j \; dS \tag{8}$$

$$B_{jk} \;\; = \;\; -\rho\int_{S_b}\text{Real}(\phi_k) \; n_j \; dS \; + \; \rho\,\frac{U}{\omega_e} \; \int_{S_b} \; \text{Imag}\left(\frac{\partial\phi_k}{\partial x}\right) \; n_j \; dS \tag{9}$$

At zero and infinite frequency limits, the real part of the velocity potential goes to zero, and the velocity potential can be represented in terms of normalized real quantities as follows:

$$\phi(\omega_e) \;\; = \;\; i \; \phi'(0) \; \omega_e \; \text{for} \; \omega_e \rightarrow 0 \tag{10}$$

$$\phi(\omega_e) \;\; = \;\; i \; \phi'(\infty) \; \omega_e \; \text{for} \; \omega_e \rightarrow \infty \tag{11}$$

At these limits the added mass and damping can be evaluated as:

$$A_{jk} \;\; = \;\; -\rho \; \int_{S_b} \phi'_k n_j \; dS \tag{12}$$

$$B_{jk} \;\; = \;\; \rho \, U \; \int_{S_b} \frac{\partial\phi'_k}{\partial x} \; n_j \; dS \tag{13}$$

For pitch and yaw, the velocity potentials at forward speed include contributions from heave and sway respectively as follows:

$$\phi_5(U,\omega_e) \;\; = \;\; \phi_5(0,\omega_e) \; + \; \frac{U}{i \; \omega_e} \; \phi_3(0,\omega_e) \tag{14}$$

$$\phi_6(U,\omega_e) \;\; = \;\; \phi_6(0,\omega_e) \; - \; \frac{U}{i \; \omega_e} \; \phi_2(0,\omega_e) \tag{15}$$

Added mass and damping coefficients for pitch can be expressed as:

$$\begin{aligned} A_{j5} &= -\frac{\rho}{\omega_e}\int_{S_b} \text{Imag}\left(\phi_5(0,\omega_e)\right) n_j \; dS \; + \; \frac{\rho}{\omega_e}\,\frac{U}{\omega_e}\,\int_{S_b} \text{Real}\left(\phi_3\right) n_j \; dS \\ &\quad - \frac{\rho}{\omega_e}\,\frac{U}{\omega_e}\,\int_{S_b} \text{Real}\left(\frac{\partial \phi_5(0,\omega_e)}{\partial x}\right) n_j \; dS \\ &\quad - \frac{\rho}{\omega_e}\,\left(\frac{U}{\omega_e}\right)^2 \int_{S_b} \text{Imag}\left(\frac{\partial \phi_3}{\partial x}\right) n_j \; dS \end{aligned} \tag{16}$$

$$\begin{aligned} B_{j5} &= -\rho\int_{S_b} \text{Real}(\phi_5(0,\omega_e)) \; n_j \; dS \; - \; \rho\frac{U}{\omega_e}\,\int_{S_b} \text{Imag}\left(\phi_3\right) \; n_j \; dS \\ &\quad + \rho\,\frac{U}{\omega_e}\,\int_{S_b} \text{Imag}\left(\frac{\partial \phi_5(0,\omega_e)}{\partial x}\right) \; n_j \; dS \\ &\quad - \rho\,\left(\frac{U}{\omega_e}\right)^2 \int_{S_b} \text{Real}\left(\frac{\partial \phi_3}{\partial x}\right) n_j \; dS \end{aligned} \tag{17}$$

At the zero and upper frequency limits, the above equations can be re-written as:

$$A_{j5} \;=\; -\rho\,\int_{S_b} (\phi_5')n_j \; dS \; - \; \rho\,\left(\frac{U}{\omega_e}\right)^2 \int_{S_b} \frac{\partial \phi_3'}{\partial x} n_j \; dS \tag{18}$$

$$B_{j5} \;=\; -\rho\,U\,\int_{S_b} (\phi_3')n_j \; dS \; + \; \rho\,U\,\int_{S_b} \frac{\partial \phi_5'}{\partial x}\; n_j \; dS \tag{19}$$

For yaw motion, added mass and damping terms are:

$$\begin{aligned} A_{j6} &= -\frac{\rho}{\omega_e}\,\int_{S_b} \text{Imag}\left(\phi_6(0,\omega_e)\right) n_j \; dS \; - \; \frac{\rho}{\omega_e}\,\frac{U}{\omega_e}\,\int_{S_b} \text{Real}\left(\phi_2\right) n_j \; dS \\ &\quad - \frac{\rho}{\omega_e}\,\frac{U}{\omega_e}\,\int_{S_b} \text{Real}\left(\frac{\partial \phi_6(0,\omega_e)}{\partial x}\right) n_j \; dS \\ &\quad + \frac{\rho}{\omega_e}\,\left(\frac{U}{\omega_e}\right)^2 \int_{S_b} \text{Imag}\left(\frac{\partial \phi_2}{\partial x}\right) n_j \; dS \end{aligned} \tag{20}$$

$$\begin{aligned} B_{j6} &= -\rho\int_{S_b} \text{Real}(\phi_6(0,\omega_e)) \; n_j \; dS \; + \; \rho\frac{U}{\omega_e}\,\int_{S_b} \text{Imag}\left(\phi_2\right) \; n_j \; dS \\ &\quad + \rho\,\frac{U}{\omega_e}\,\int_{S_b} \text{Imag}\left(\frac{\partial \phi_6(0,\omega_e)}{\partial x}\right) \; n_j \; dS \\ &\quad + \rho\,\left(\frac{U}{\omega_e}\right)^2 \int_{S_b} \text{Real}\left(\frac{\partial \phi_2}{\partial x}\right) n_j \; dS \end{aligned} \tag{21}$$

Yaw motion terms at the zero and upper frequency limits are:

$$A_{j6} \;=\; -\rho\,\int_{S_b} (\phi_6')n_j \; dS \; + \; \rho\,\left(\frac{U}{\omega_e}\right)^2 \int_{S_b} \frac{\partial \phi_2'}{\partial x} n_j \; dS \tag{22}$$

$$B_{j6} \;=\; \rho\,U\,\int_{S_b} (\phi_2')n_j \; dS \; + \; \rho\,U\,\int_{S_b} \frac{\partial \phi_6'}{\partial x}\; n_j \; dS \tag{23}$$

For computational purposes, it is useful to be able to express ship hydrodynamic coefficients at forward speed as functions of zero speed coefficients as follows:

$$A_{jk}(U,\omega_e) = A_{jk}(0,\omega_e) + \frac{U}{\omega_e^2}\frac{\partial B_{jk}(0,\omega_e)}{\partial x} \quad \text{for } k = 1-4 \tag{24}$$

$$B_{jk}(U,\omega_e) = B_{jk}(0,\omega_e) - U\frac{\partial A_{jk}(0,\omega_e)}{\partial x} \quad \text{for } k = 1-4 \tag{25}$$

$$\begin{aligned} A_{j5}(U,\omega_e) &= A_{j5}(0,\omega_e) - \frac{U}{\omega_e^2}B_{j3}(0,\omega_e) + \frac{U}{\omega_e^2}\frac{\partial B_{j5}(0,\omega_e)}{\partial x} \\ &\quad + \left(\frac{U}{\omega_e}\right)^2\frac{\partial A_{j3}(0,\omega_e)}{\partial x} \end{aligned} \tag{26}$$

$$\begin{aligned} B_{j5}(U,\omega_e) &= B_{j5}(0,\omega_e) + U\,A_{j3}(0,\omega_e) - U\frac{\partial A_{j5}(0,\omega_e)}{\partial x} \\ &\quad + \left(\frac{U}{\omega_e}\right)^2\frac{\partial B_{j3}(0,\omega_e)}{\partial x} \end{aligned} \tag{27}$$

$$\begin{aligned} A_{j6}(U,\omega_e) &= A_{j6}(0,\omega_e) + \frac{U}{\omega_e^2}B_{j2}(0,\omega_e) + \frac{U}{\omega_e^2}\frac{\partial B_{j6}(0,\omega_e)}{\partial x} \\ &\quad - \left(\frac{U}{\omega_e}\right)^2\frac{\partial A_{j2}(0,\omega_e)}{\partial x} \end{aligned} \tag{28}$$

$$\begin{aligned} B_{j6}(U,\omega_e) &= B_{j6}(0,\omega_e) - U\,A_{j2}(0,\omega_e) - U\frac{\partial A_{j6}(0,\omega_e)}{\partial x} \\ &\quad - \left(\frac{U}{\omega_e}\right)^2\frac{\partial B_{j2}(0,\omega_e)}{\partial x} \end{aligned} \tag{29}$$

The above equations are the basis for a ship hydrodynamic coefficient database which gives coefficients at arbitrary forward speed based on stored coefficients for zero forward speed.

3 Hydrodynamic Forces for Transient Motions

The hydrodynamic forces for transient motions of floating bodies are discussed in several references. Mei [2] and Wehausen [3] give comprehensive overviews. McTaggart [4] discusses transient motions of icebergs during drifting and collisions with offshore structures. Magee [5] gives a good overview of transient hydrodynamic forces acting on ships, and includes forward speed effects. Fonseca and Guedes Soares [6] present theory and results for time domain ship motions based on frequency domain coefficients.

For a floating body undergoing transient motions, the equations of motion can be

expressed as:

$$([M] + [A(U,\infty)])\ \{\ddot{\eta}(t)\}\ +\ [b(U)]\ \left\{\dot{\eta(t)}\right\} + \int_{-\infty}^{t} [K(U,t-\tau)]\,\{\dot{\eta}(\tau)\}\ d\tau + ([C]\ +\ [c(U)])\ \{\eta(t)\}\ =\ \left\{F^I(t)\ +\ F^D(t)\right\} \quad (30)$$

where $[b(U)]$ is the speed dependent damping matrix in the time domain, $[K(U,t-\tau)]$ is the retardation function matrix for delay time $t-\tau$, and $[c(U)]$ is the speed dependent stiffness matrix in the time domain. Terms in the above equation can be evaluated using results from frequency domain computations.

3.1 Retardation Functions

The retardation functions $K_{jk}(U,\tau)$ can be determined from frequency domain added mass or damping coefficients as follows:

$$K_{jk}(\tau) = -\frac{2}{\pi}\int_0^\infty [A_{jk}(U,\omega_e)\ -\ A_{jk}(U,\infty)]\ \omega_e\ \sin\omega_e\tau\ d\omega_e \quad (31)$$

$$K_{jk}(\tau) = \frac{2}{\pi}\int_0^\infty B_{jk}(U,\omega_e)\ \cos\omega_e\tau\ d\omega_e \quad (32)$$

When selecting between the above two equations for evaluating retardation functions, it should be noted that damping coefficients approach their infinite frequency limits much more quickly than do added masses. Given the problems with irregular frequencies that can occur at higher frequencies, it was decided to compute retardation functions based on damping where possible. Fonseca and Guedes Soares present a similar approach based on hydrodynamic coefficients evaluated using strip theory.

It is convenient to express retardation functions in terms of speed-independent and speed-dependent terms. For modes for which velocity potentials are assumed to be independent of ship speed (i.e., surge, sway, heave, and roll), the retardation functions can be expressed as:

$$K_{jk}(U,\tau) = K^0_{jk}(\tau)\ +\ U\ K^U_{jk}(\tau) \text{ for } k = 1-4 \quad (33)$$

The speed-independent retardation functions are evaluated using:

$$K^0_{ij}(\tau) = \frac{2}{\pi}\int_0^\infty B_{jk}(0,\omega_e)\ \cos\omega_e\tau\ d\omega_e \text{ for } k = 1-6 \quad (34)$$

Note that the above equation is valid for all six degrees of freedom. The speed dependent terms based on Equations (25) and (32) are:

$$K_{jk}^{U}(\tau) = -\frac{2}{\pi}\int_0^\infty \left[\frac{\partial A_{jk}(0,\omega_e)}{\partial x} - \frac{\partial A_{jk}(0,\infty)}{\partial x}\right] \cos\omega_e t \; d\omega_e \quad \text{for } k = 1-4 \tag{35}$$

For pitch and yaw, the velocity potentials are influenced by forward speed, and the retardation functions are expressed as:

$$K_{jk}(U,\tau) = K_{jk}^{0}(\tau) + U\, K_{jk}^{U}(\tau) + U^2\, K_{jk}^{UU}(\tau) \text{ for } k = 5-6 \tag{36}$$

The speed-dependent coefficients due to pitch motion are evaluated by:

$$K_{j5}^{U}(\tau) = -\frac{2}{\pi}\int_0^\infty \left[\frac{\partial A_{j5}(0,\omega_e)}{\partial x} - \frac{\partial A_{j5}(0,\infty)}{\partial x}\right] \cos\omega_e\tau \; d\omega_e + \frac{2}{\pi}\int_0^\infty B_{j3}(0,\omega_e)\,\frac{\sin\omega_e\tau}{\omega_e}\; d\omega_e \tag{37}$$

$$K_{j5}^{UU}(\tau) = \frac{2}{\pi}\int_0^\infty \frac{\partial B_{j3}(0,\omega_e)}{\partial x}\,\frac{\cos\omega_e\tau}{\omega_e^2}\; d\omega_e \tag{38}$$

When evaluating K_{j5}^{U} in Equation (37), the contribution from the heave velocity potential is evaluated using heave damping rather than added mass because it has been found to give better numerical accuracy. Both Equations (37) and (38) have integrands with encounter frequency ω_e or its square in the denominator. Fortunately, these integrands are not problematic as ω_e approaches zero because damping is zero at zero encounter frequency.

Similarly, the speed-dependent coefficients due to yaw motion are evaluated by:

$$K_{j6}^{U}(\tau) = -\frac{2}{\pi}\int_0^\infty \left[\frac{\partial A_{j6}(0,\omega_e)}{\partial x} - \frac{\partial A_{j6}(0,\infty)}{\partial x}\right] \cos\omega_e\tau \; d\omega_e - \frac{2}{\pi}\int_0^\infty B_{j2}(0,\omega_e)\,\frac{\sin\omega_e\tau}{\omega_e}\; d\omega_e \tag{39}$$

$$K_{j6}^{UU}(\tau) = -\frac{2}{\pi}\int_0^\infty \frac{\partial B_{j2}(0,\omega_e)}{\partial x}\,\frac{\cos\omega_e\tau}{\omega_e^2}\; d\omega_e \tag{40}$$

3.2 Hydrodynamic Damping and Stiffness

Hydrodynamic damping and stiffness terms are related to frequency domain values as follows:

$$b_{jk}(U) = -U\,\frac{\partial A_{jk}(0,\infty)}{\partial x} \quad \text{for } k = 1-4 \tag{41}$$

$$b_{j5}(U) = -U\,\frac{\partial A_{j5}(0,\infty)}{\partial x} + U\,A_{j3}(0,\infty) \quad (42)$$

$$b_{j6}(U) = -U\,\frac{\partial A_{j6}(0,\infty)}{\partial x} - U\,A_{j2}(0,\infty) \quad (43)$$

$$c_{j5}(U) = -U^2\,\frac{\partial A_{j3}(0,0)}{\partial x} \quad (44)$$

$$c_{j6}(U) = U^2\,\frac{\partial A_{j2}(0,0)}{\partial x} \quad (45)$$

Note that the two stiffness terms arise from converting frequency domain added mass terms to stiffness terms using multiplication by $-\omega_e^2$. The stiffness terms are based on sway and heave added masses at zero frequency.

3.3 Wave Excitation Forces

Linear wave excitation forces in the time domain can be evaluated using the frequency domain forces presented in Reference 1. For a linear wave system, the incident wave elevation in the time domain can be expressed as:

$$\zeta_I(x,y,t) = a\,\cos\left[\omega_e\,t + \epsilon_I - k_I\,(x\cos\beta - y\sin\beta)\right] \quad (46)$$

where a is incident wave amplitude, ϵ_I is the phase of the incident wave crest (positive for time lead) at the origin, k_I is the incident wavenumber, and β is the incident wave direction. Wave excitation forces in the time domain can be expressed in terms of frequency domain values as follows:

$$F_j^I(t) = \left|F^I(U,\beta,\omega_I)\right|\,\cos\left[\omega_e t + \epsilon_I + \epsilon\left(F^I(U,\beta,\omega_I)\right)\right] \quad (47)$$

$$F_j^D(t) = \left|F^D(U,\beta,\omega_I)\right|\,\cos\left[\omega_e t + \epsilon_I + \epsilon\left(F^D(U,\beta,\omega_I)\right)\right] \quad (48)$$

where $F^I(U,\beta,\omega_I)$ is the complex incident excitation force in the frequency domain and $F^D(U,\beta,\omega_I)$ is the complex diffraction excitation force in the frequency domain. The phases of the incident and diffracted excitation forces for incident waves with zero phase angles are given by:

$$\epsilon\left(F^I(U,\beta,\omega_I)\right) = \arctan\frac{\text{Imag}\left\{F^I(U,\beta,\omega_I)\right\}}{\text{Real}\left\{F^I(U,\beta,\omega_I)\right\}} \quad (49)$$

$$\epsilon\left(F^D(U,\beta,\omega_I)\right) = \arctan\frac{\text{Imag}\left\{F^D(U,\beta,\omega_I)\right\}}{\text{Real}\left\{F^D(U,\beta,\omega_I)\right\}} \quad (50)$$

4 CPF Hydroelastic Model Hull for Sample Computations of Hydrodynamic Coefficients

To demonstrate results of computations this report uses the HALIFAX class, also known as the Canadian Patrol Frigate (CPF). To enable comparison of motion predictions with model test results, the loading condition for the present computations is the deep departure condition for the CPF hydroelastic model, as described in Reference 7. Note that a slightly different loading condition was used for sample computations of frequency domain coefficients in Reference 1.

Table 1 gives the main particulars. Three different hydrodynamic meshes have been generated, as shown in Figures 3 to 5. The panel colours in each figure represent depth below the waterline. Table 2 gives hydrostatic properties computed using each mesh. Preliminary hydrodynamic computations indicated that the x derivative of added mass was somewhat sensitive to the limiting aspect ratio (lenghtwise/girthwise) used for panelling the hull. Limiting aspect ratios of 3 and 5 were tested, with a value of 3 being ultimately chosen due to better convergence of results with increasing number of panels.

Table 1: *Main Particulars for HALIFAX Class Frigate, CPF Hydroelastic Model Deep Departure Condition*

Length, L	124.5 m
Beam, B	14.8 m
Midships draft, T_{mid}	4.97 m
Trim by stern, t_s	-0.04 m
Displacement, $\triangle$	4655 tonnes (fresh water)
Vertical centre of gravity, $\overline{KG}$	6.26 m
Dry roll radius of gyration r_{xx}	5.82 m
Dry pitch radius of gyration r_{yy}	28.8 m
Dry yaw radius of gyration r_{zz}	28.8 m

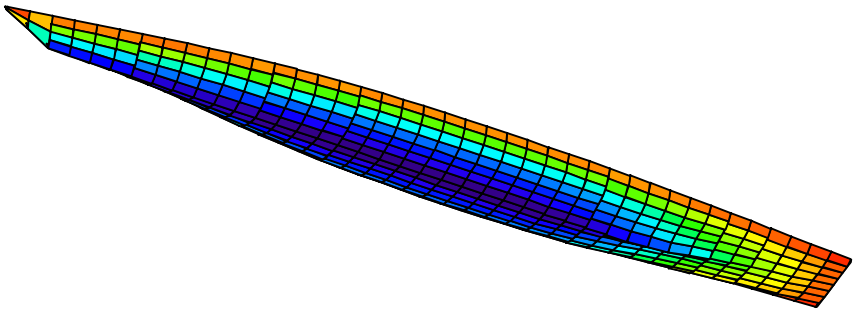

Figure 3: *Coarse Mesh for CPF Hydroelastic Model*

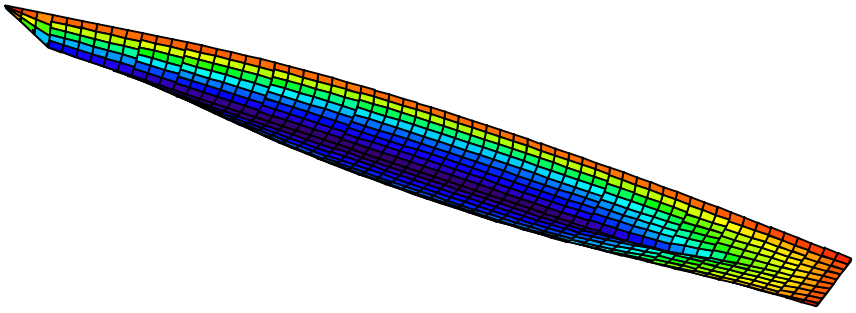

Figure 4: *Medium Mesh for CPF Hydroelastic Model*

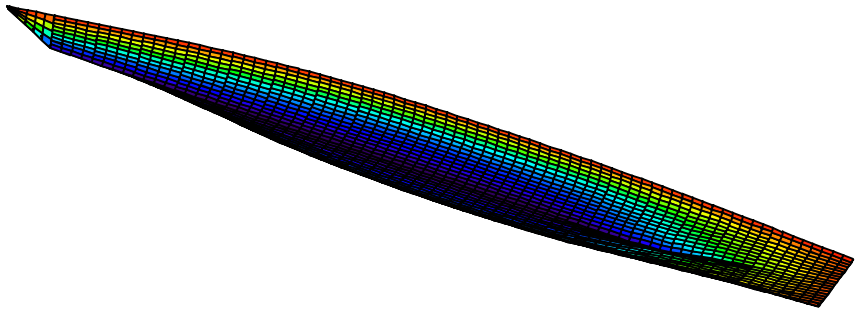

Figure 5: *Fine Mesh for CPF Hydroelastic Model*

Table 2: *Hydrostatic Properties for Different Panel Meshes*

	Coarse	Medium	Fine
Nominal panel size (m^2)	5.0	2.5	1.0
Number of panels on port side N_p^{port}	224	433	1040
Volume (m^3)	4465.8	4488.8	4500.6
LCB aft of FP (m)	64.663	64.665	64.678
CB wrt waterline (m)	-1.882	-1.889	-1.893
Wetted surface area (m^2)	1965.6	1969.4	1971.2

5 Improvements to Computations of Frequency Domain Coefficients

The present approach for computing time domain hydrodynamic coefficients requires accurate and efficient computation of frequency domain coefficients. This section presents several improvements that have been made to computations of frequency domain coefficients subsequent to the work reported in Reference 1.

5.1 Maintenance of Points on Waterline During Panel Transformation

The wetted surface of a hull is represented using triangular and quadrilateral panels. As discussed in Reference 1, it is usually necessary to make slight modifications to points of quadrilateral panels to ensure that all points lie in the same plane. Panelling computations have been changed such that a panel point located on the hull waterline remains on the waterline $z_{wl} = 0$, with only x and y coordinates being changed to obtain a planar panel. This modification prevents numerical inconsistencies which can occur when panel points are located above the waterline.

5.2 Sign Correction to Speed Dependent Added Mass

As stated in Section 2, Equation 9 of Reference 1 contained a sign error for the speed dependent term of added mass. Equation (6) gives the correct added mass.

5.3 Improved Accuracy for x Derivatives of Velocity Potential

Improved accuracy has been introduced for evaluating the x derivatives of velocity potential. The following equation is still used for computing the x derivatives:

$$\left\{ \frac{\partial \phi}{\partial x} \right\} \;=\; [H] \; \{\sigma\} \tag{51}$$

where $[H]$ is the influence matrix and $\{\sigma\}$ is the vector of source strengths. The influence matrix coefficients were previously evaluated as follows:

$$H_{jk} \;=\; -\delta_{jk} \, \frac{1}{2} \, n_{x-j} \;+\; (1 \;-\; \delta_{jk}) \, \frac{1}{4\pi} \int_{S_k} \frac{\partial (1/R(\vec{x}_j, \vec{x}_s))}{\partial x_{\vec{x}_j}} \, dS$$

$$
\begin{aligned}
&+ \frac{1}{4\pi} \int_{S_k} \frac{\partial(1/R_1(\vec{x}_j, \vec{x}_s))}{\partial x_{\vec{x}_j}} \, dS \\
&+ \frac{1}{4\pi} \int_{S_k} \frac{\partial \widetilde{G}_0(\vec{x}_j, \vec{x}_s)}{\partial x_{\vec{x}_j}} \, dS \qquad \text{for } \omega_e \leq \omega_e^t \qquad (52) \\
H_{jk} \;=\; & -\delta_{jk} \frac{1}{2} \, n_{x-j} \, + \, (1 \, - \, \delta_{jk}) \, \frac{1}{4\pi} \int_{S_k} \frac{\partial(1/R(\vec{x}_j, \vec{x}_s))}{\partial x_{\vec{x}_j}} \, dS \\
&- \frac{1}{4\pi} \int_{S_k} \frac{\partial(1/R_1(\vec{x}_j, \vec{x}_s))}{\partial x_{\vec{x}_j}} \, dS \\
&+ \frac{1}{4\pi} \int_{S_k} \frac{\partial \widetilde{G}_\infty(\vec{x}_j, \vec{x}_s)}{\partial x_{\vec{x}_j}} \, dS \qquad \text{for } \omega_e > \omega_e^t \qquad (53)
\end{aligned}
$$

where n_{x-j} is the x component of the outward normal on panel j, δ_{jk} is the Kroenecker delta function, S_k is the surface of source panel k, $R(\vec{x}_j, \vec{x}_s)$ is the radius from field point $\vec{x}_j$ to source panel point $\vec{x}_s$, R_1 is the radius from the field point to the image of the source panel point, $\widetilde{G}_0$ is the frequency dependent Green function relative to the zero frequency Green function, ω_e^t is the transition encounter frequency for indicating which form of the frequency dependent Green function to use, and $\widetilde{G}_\infty$ is the frequency dependent Green function relative to the infinite frequency Green function. The selection of which of the above equations to use depends upon a specified transition encounter frequency ω_e^t. For the case $j = k$ considering the flow from a source panel on itself, the above equations are based on the following assumption:

$$
\int_{S_k} \frac{\partial(1/R(\vec{x}_j, \vec{x}_s))}{\partial x_{\vec{x}_j}} \, dS \;\approx\; -2 \, \pi \, n_{x-j} \qquad \text{for } j = k \qquad (54)
$$

Although this equation is a good approximation, it has been found that it should not be used because computed x derivatives of velocity potentials can be very sensitive to small differences in influence coefficients H_{jk}. Consequently, the influence coefficients are now evaluated by:

$$
\begin{aligned}
H_{jk} \;=\; & \frac{1}{4\pi} \int_{S_k} \frac{\partial(1/R(\vec{x}_j, \vec{x}_s))}{\partial x_{\vec{x}_j}} \, dS + \frac{1}{4\pi} \int_{S_k} \frac{\partial(1/R_1(\vec{x}_j, \vec{x}_s))}{\partial x_{\vec{x}_j}} \, dS \\
&+ \frac{1}{4\pi} \int_{S_k} \frac{\partial \widetilde{G}_0(\vec{x}_j, \vec{x}_s)}{\partial x_{\vec{x}_j}} \, dS \qquad \text{for } \omega_e \leq \omega_e^t \qquad (55) \\
H_{jk} \;=\; & \frac{1}{4\pi} \int_{S_k} \frac{\partial(1/R(\vec{x}_j, \vec{x}_s))}{\partial x_{\vec{x}_j}} \, dS \; - \; \frac{1}{4\pi} \int_{S_k} \frac{\partial(1/R_1(\vec{x}_j, \vec{x}_s))}{\partial x_{\vec{x}_j}} \, dS \\
&+ \frac{1}{4\pi} \int_{S_k} \frac{\partial \widetilde{G}_\infty(\vec{x}_j, \vec{x}_s)}{\partial x_{\vec{x}_j}} \, dS \qquad \text{for } \omega_e > \omega_e^t \qquad (56)
\end{aligned}
$$

5.4 Gauss Quadrature for Integration from Source Panel

When integrating the Green function from a source panel, the frequency dependent portion was previously approximated using the centroid of the source panel. A new option has been introduced for using Gauss quadrature (see Cook [8]) on source panels for integrating the frequency dependent portion of the Green function. The new implementation has options for using 1, 4, or 9 quadrature points per source panel.

5.5 Galerkin Method for Evaluation of Velocity Potential Influence Coefficients

Previous computations of influence matrices were based on the velocity potential at the centroid of each panel. The Galerkin approach allows influence matrix terms to be based on weighted values of the Green function evaluated at 1, 4, or 9 quadrature points on each field panel. Sclavounos and Lee [9] give a detailed discussion of this approach.

The accuracy of computed velocity potentials will increase with the number of quadrature points used with the Galerkin method and for integrating the frequency dependent portion of the Green function from source panels. This increased accuracy comes at the expense of higher computation times due to larger numbers of computations of Green functions. Figure 6 shows heave damping and added mass x derivative for two different sets of computations. The first set of computations uses 4 quadrature points per panel applied to the Galerkin method and integration of the frequency dependent term from source panels. The second set of computations is based on centroid approximations. At higher frequencies (the first irregular frequency and higher), the numerical results are sensitive to accuracy of influence coefficients; thus, the higher order computations give better results, particularly for the x derivative of added mass.

5.6 Additional C Code for Faster Computations

As discussed in Reference 1, most of the present numerical predictions have been developed in Python [10], a high-level, interpreted computer language. When developing Python applications, it is common practice to determine which portions are CPU intensive and to re-write them in C to obtain the performance of compiled, optimized code. Previously, the frequency dependent portion of the Green function was written in C. New C code has been developed to evaluate the frequency independent terms of the Green function. In addition, a new C function has been

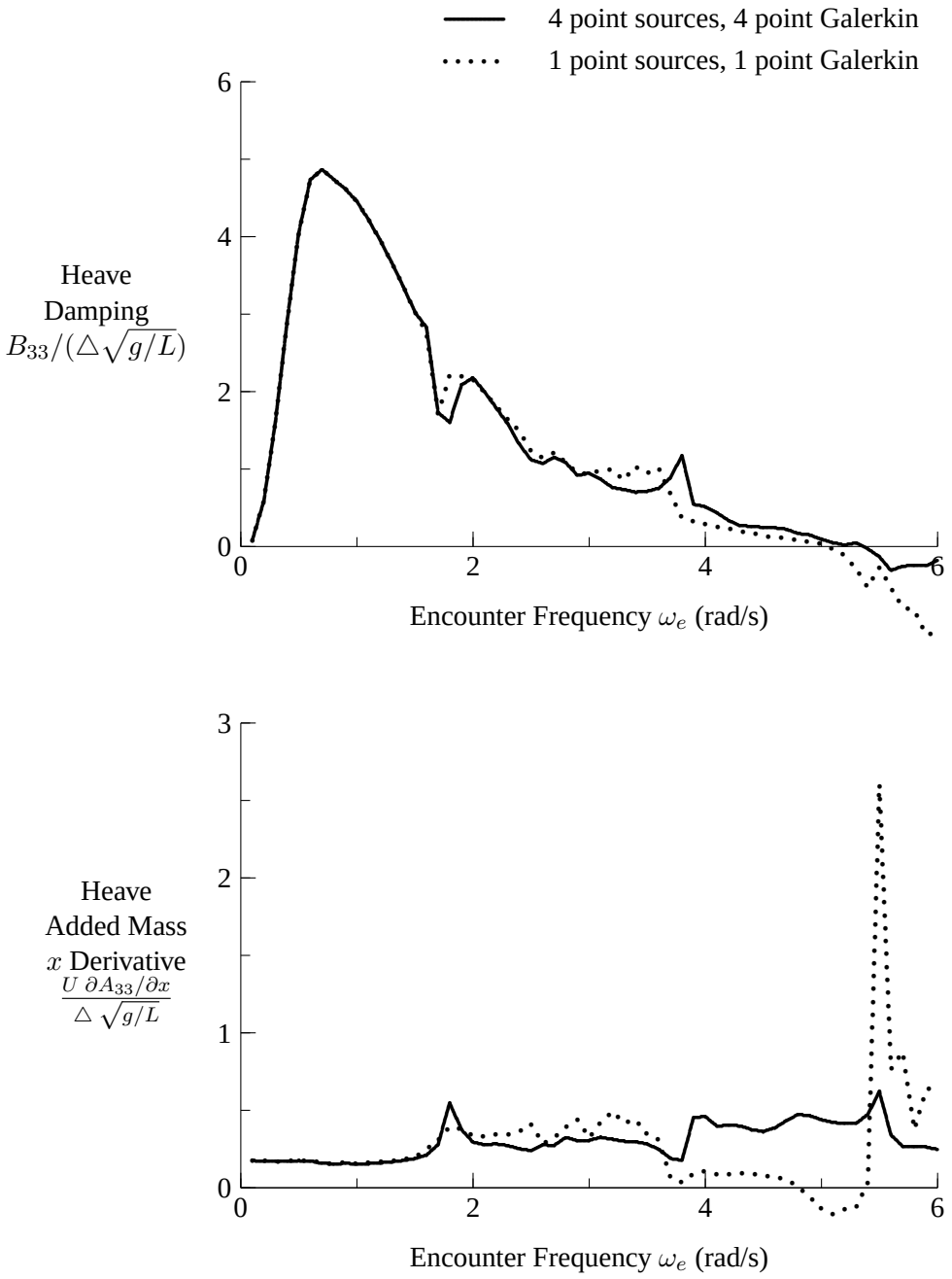

Figure 6: *Dimensionless Forces from Zero Speed Heave Damping and x Derivative for HALIFAX at 20 Knots, Medium Mesh, with Centroid and Four Point Approximations*

developed to evaluate influence matrices for the frequency dependent portion of the Green function given input vectors of panel points.

5.7 Removal of Irregular Frequencies from Database

Computations of hydrodynamic coefficients can be adversely influenced by irregular frequencies, at which mathematical solutions of velocity potentials are incorrect. McTaggart [11] and Ando [12] discuss the occurrence of irregular frequencies in detail.

For modelling and simulation work, it is likely that hydrodynamic coefficients will typically be determined using interpolation from a previously generated database of hydrodynamic coefficients. The accuracy of interpolated coefficients will be improved if the database does not have hydrodynamic coefficients adversely affected by irregular frequencies. Fortunately, a method is available for indicating likely irregular frequencies which should be excluded from the database. As was presented in Reference 1, radiation source strengths on the port side of a symmetrical hull can be solved by satisfying the following:

$$[D^{even}] \left\{\sigma_j^{port}\right\} = \left\{\partial\phi_j^{port}/\partial n\right\} \text{ for } j = 1,3,5 \quad (57)$$

$$\left[D^{odd}\right] \left\{\sigma_j^{port}\right\} = \left\{\partial\phi_j^{port}/\partial n\right\} \text{ for } j = 2,4,6 \quad (58)$$

where $[D^{even}]$ is the influence matrix for normal velocity on the hull port side due to sources on the port side when velocity potential is an even function of y, $\left\{\sigma_j^{port}\right\}$ is the vector of source strengths on the port side for motion mode j, $\left\{\partial\phi_j^{port}/\partial n\right\}$ is the vector of hull normal velocities on the port side, and $\left[D^{odd}\right]$ is the influence matrix for normal velocity on the hull port side due to sources on the port side when velocity potential is an odd function of y. The normal velocity influence matrices are given by:

$$[D^{even}] = \left[D^{port,port}\right] + \left[D^{port,star}\right] \quad (59)$$

$$\left[D^{odd}\right] = \left[D^{port,port}\right] - \left[D^{port,star}\right] \quad (60)$$

where $\left[D^{port,port}\right]$ is the influence matrix for normal velocities on the port side due to sources on the port side and $[D^{port,star}]$ is the influence matrix for normal velocities on the port side due to sources on the starboard side.

As suggested by Lee and Sclavounos [13], irregular frequencies are indicated by high condition numbers for the influence matrices $[D^{even}]$ and $\left[D^{odd}\right]$ for their respective motion modes. The condition number for a matrix $[D]$ can be computed as follows [14]:

$$\lambda = ||[D]|| \times \left|\left|\left[D^{-1}\right]\right|\right| \quad (61)$$

where $||[D]||$ is the norm of matrix $[D]$ and $\left|\left|[D]^{-1}\right|\right|$ is the norm of its inverse. The norm of $[D]$ is given by:

$$||[D]|| \quad = \quad \max \sum_{k=1}^{N} |D_{jk}| \tag{62}$$

and the norm of $[D]^{-1}$ is evaluated in a similar manner. The most computationally intensive aspect of using the above equation is evaluation of the inverse $[D^{-1}]$. Fortunately, this is not a big obstacle when evaluating hydrodynamic coefficients because the number of degrees of freedom is typically less than 2000. Furthermore, the computed inverse can be used for computing source strengths using direct matrix multiplication.

Figures 7 to 12 show normalized hydrodynamic coefficients and matrix condition numbers for the HALIFAX using coarse, medium, and fine panel meshes. The figures demonstrate that local maxima of matrix condition numbers can be indicators of irregular frequencies. To reduce irregular frequency effects, envelopes of maximum allowable matrix condition numbers can be provided as input for numerical computations. For a given hull panel mesh, separate envelopes are provided for longitudinal and lateral modes. If the computed matrix condition number for a given encounter frequency exceeds the specified envelope, then computations for that encounter frequency are not used. To determine appropriate condition number envelopes, initial computations of hydrodynamic coefficients and condition numbers are required, followed by examination of results such as those given in Figures 7 to 12. Note that the condition number envelopes will depend upon the underwater hull geometry, and to a lesser extent upon the hull panel size used.

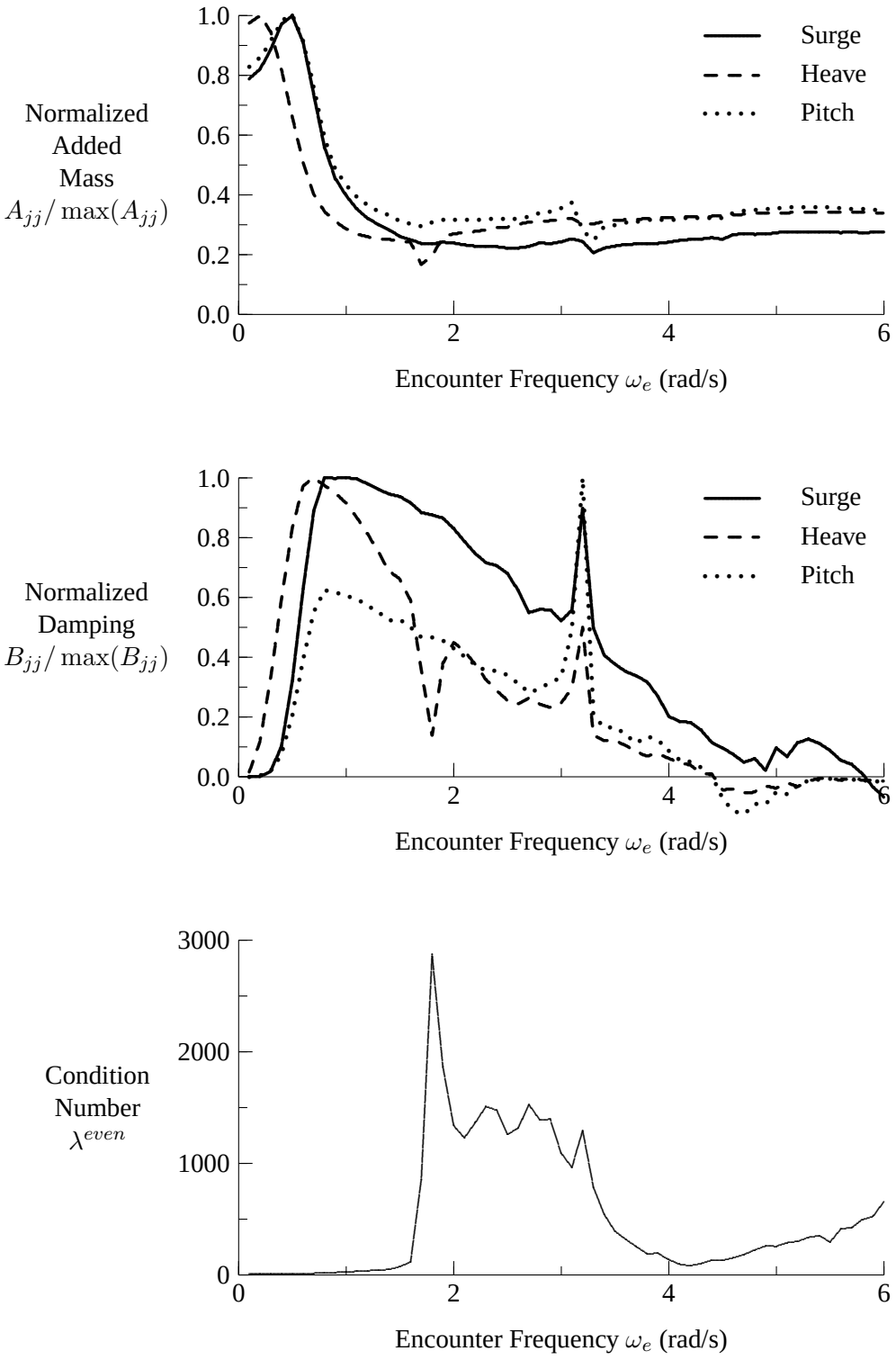

Figure 7: *Normalized Added Mass and Damping, and Normal Velocity Condition Number for HALIFAX Coarse Mesh, Longitudinal Modes*

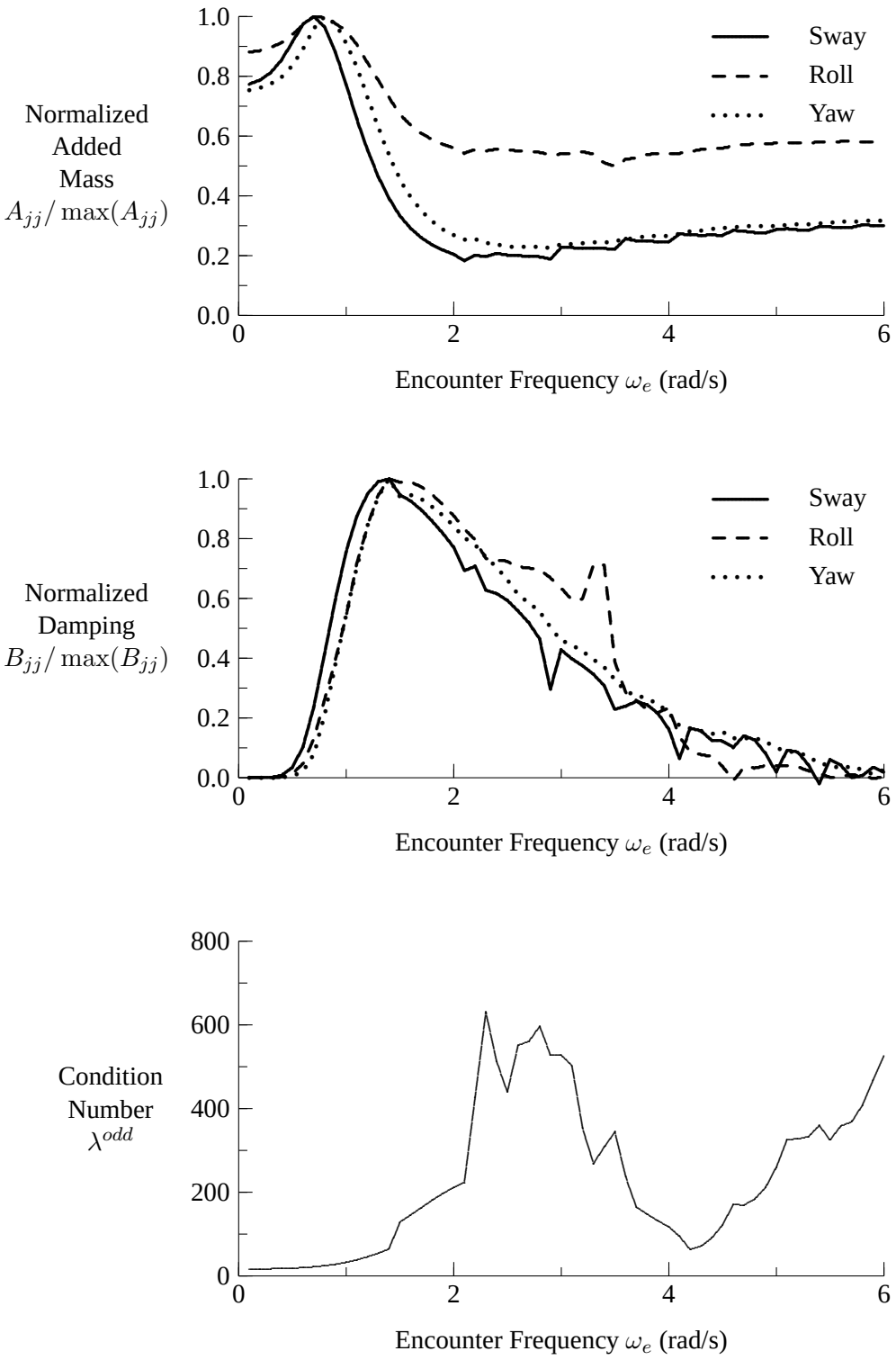

Figure 8: *Normalized Added Mass and Damping, and Normal Velocity Condition Number for HALIFAX Coarse Mesh, Lateral Modes*

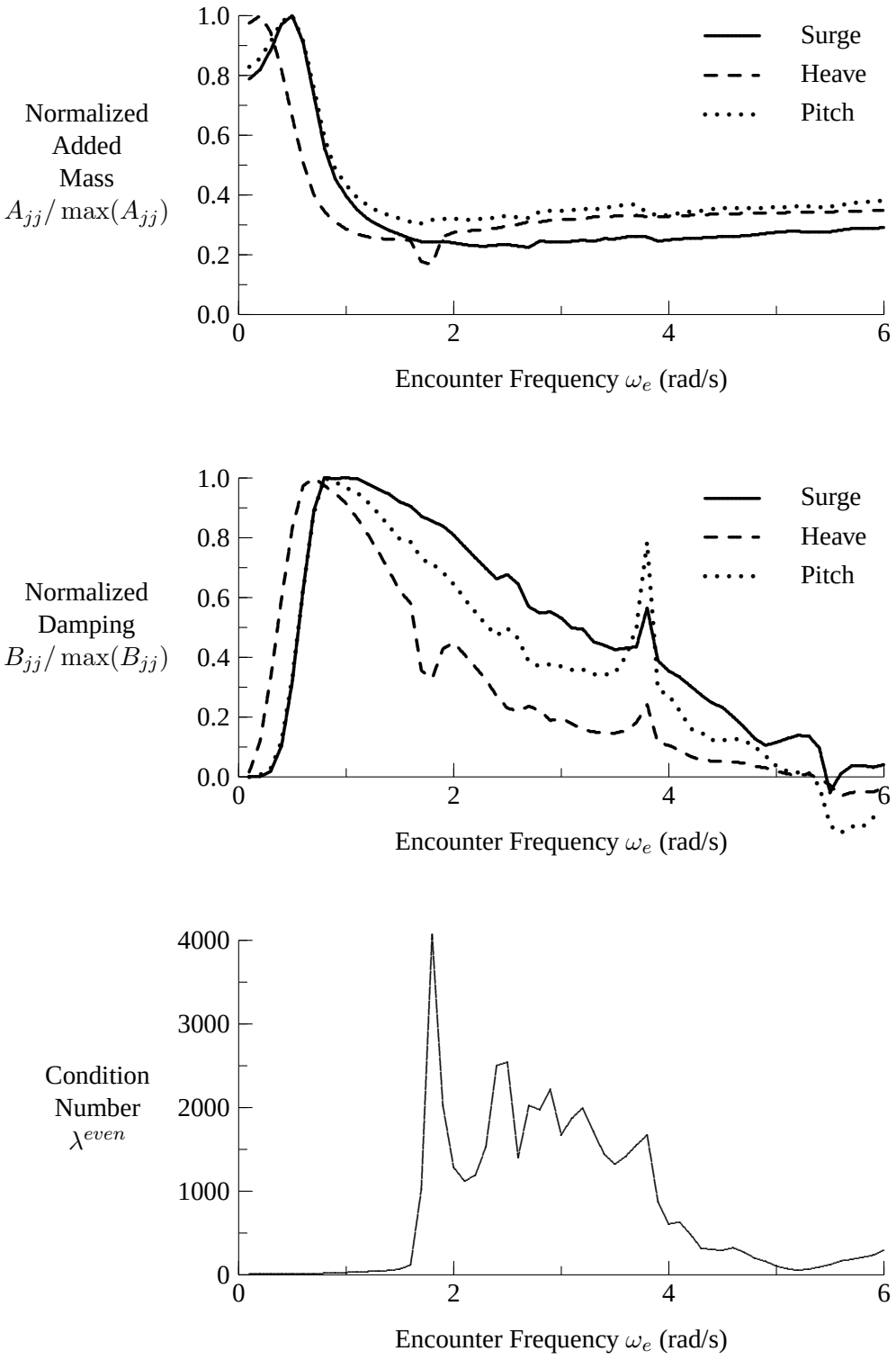

Figure 9: *Normalized Added Mass and Damping, and Normal Velocity Condition Number for HALIFAX Medium Mesh, Longitudinal Modes*

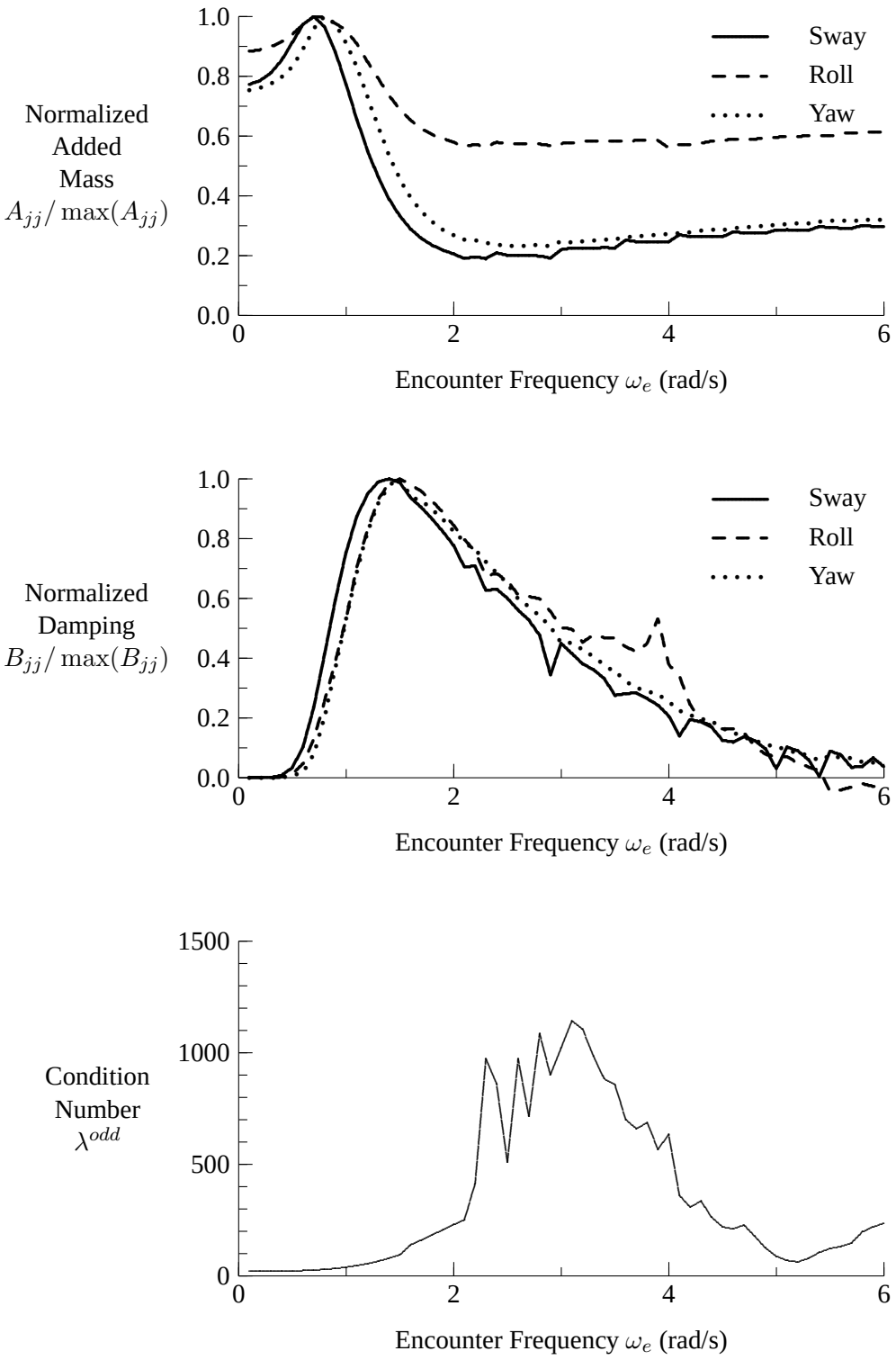

Figure 10: *Normalized Added Mass and Damping, and Normal Velocity Condition Number for HALIFAX Medium Mesh, Lateral Modes*

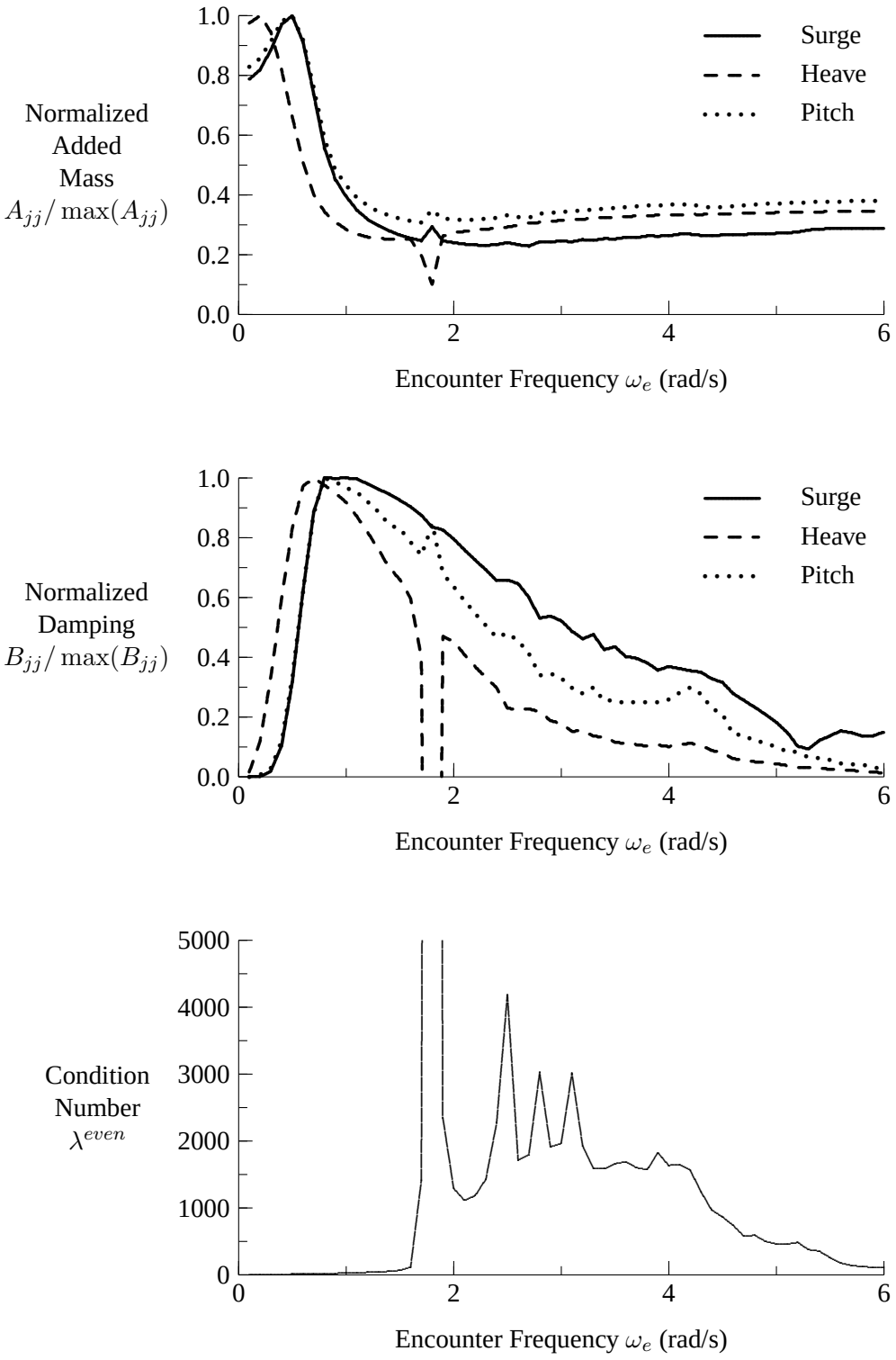

Figure 11: *Normalized Added Mass and Damping, and Normal Velocity Condition Number for HALIFAX Fine Mesh, Longitudinal Modes*

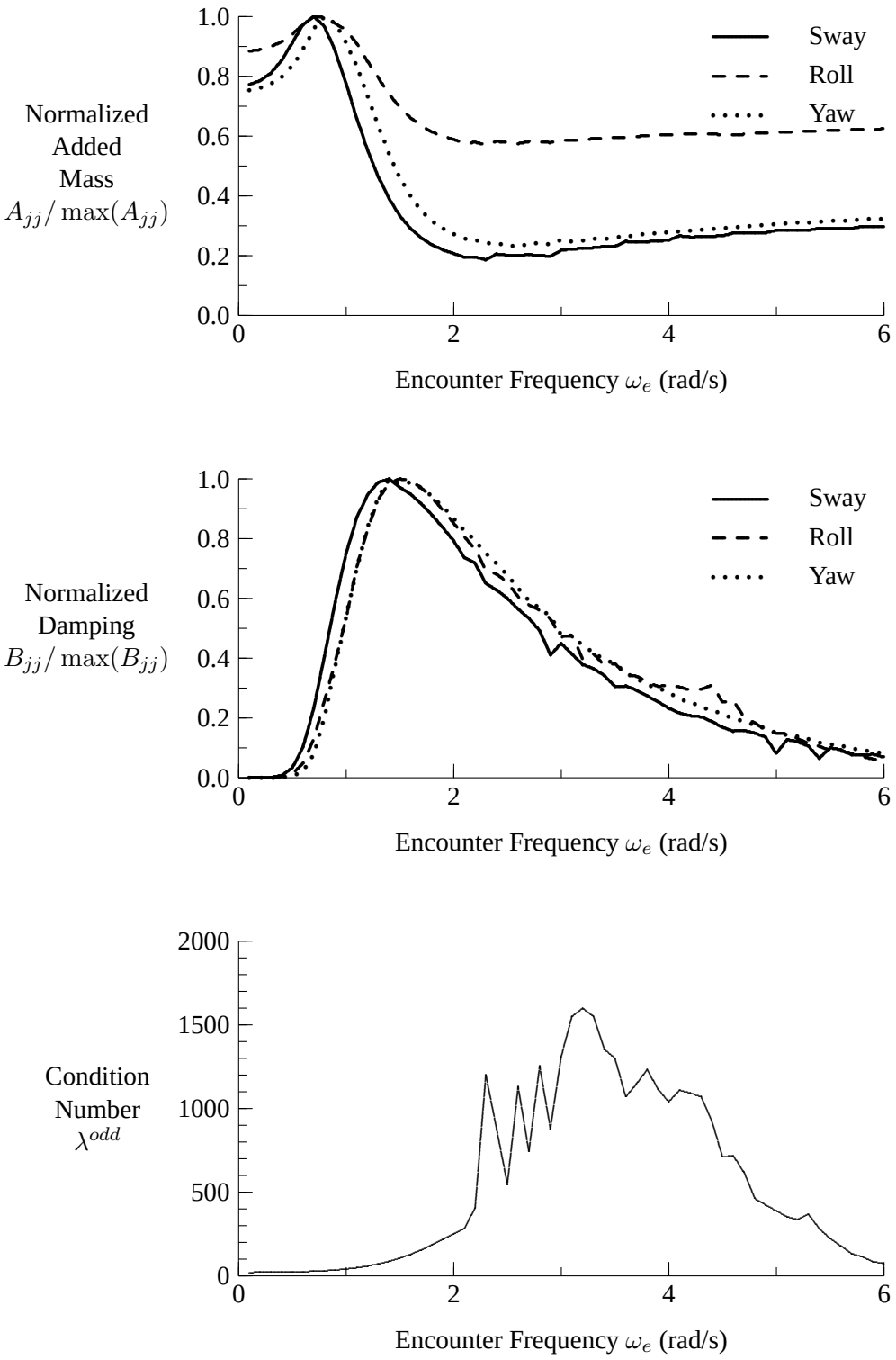

Figure 12: *Normalized Added Mass and Damping, and Normal Velocity Condition Number for HALIFAX Fine Mesh, Lateral Modes*

5.8 Direct Evaluation of Incident Wave Forces in Database of Radiation and Wave Excitation Forces

Reference 1 introduced a database class of radiation and wave excitation forces in the frequency domain. This database stored computed values for added mass, damping, incident wave force, and diffracted wave force. Using the stored values, added mass and damping could then be quickly evaluated through linear interpolation based on encounter frequency. Similarly, incident and diffracted wave forces in unit amplitude waves could be quickly evaluated through linear interpolation based on ship speed, relative sea direction, and wave frequency.

The database class has been revised such that incident wave forces are now evaluated directly rather than obtained by interpolation of stored forces. Direct evaluation of incident wave forces requires relatively little computation time; thus, this revision increases accuracy at very little computational expense. Furthermore, incident wave forces are usually greater in magnitude than diffracted wave forces, so the improvement provides a significant increase in the accuracy of wave excitation forces.

5.9 Improved Efficiency for Evaluating Diffracted Wave Potentials

A new computational approach has been introduced for evaluating diffracted wave potentials. Recall that diffraction source strengths potentials are solved as follows:

$$[D]\ \{\sigma_D\} \ = \ -\ \left\{\frac{\partial \phi_I}{\partial n}\right\} \tag{63}$$

where $[D]$ is the influence coefficient matrix relating hull normal velocity to source strength, $\{\sigma_D\}$ is the vector of hull diffraction source strengths, and $\{\partial\phi_I/\partial n\}$ is the vector of incident wave normal velocities. The above equation is based on sources distributed over the entire submerged portion of the hull (i.e., both port and starboard sides). The incident wave potential is given by:

$$\phi_I \ = \ \frac{i\ g\ a}{\omega_I}\ \exp\left[-i\ k_I\ (x\cos\beta\ -\ y\sin\beta)\right]\ \exp(k_I\ z_{wl}) \tag{64}$$

Equation (64) is based on the convention of the wave crest being at the $x-y$ origin at time $t=0$. Fluid velocities are given by the following derivatives:

$$\frac{\partial \phi_I}{\partial x} \ = \ a\ \omega_I\ \cos\beta\ \exp\left[-i\ k_I\ (x\cos\beta\ -\ y\sin\beta)\right]\ \exp(k_I\ z_{wl}) \tag{65}$$

$$\frac{\partial \phi_I}{\partial y} = -a\,\omega_I\,\sin\beta\,\exp\left[-i\,k_I\,(x\cos\beta\,-\,y\sin\beta)\right]\,\exp(k_I\,z_{wl}) \quad (66)$$

$$\frac{\partial \phi_I}{\partial z} = i\,a\,\omega_I\,\exp\left[-i\,k_I\,(x\cos\beta\,-\,y\sin\beta)\right]\,\exp(k_I\,z_{wl}) \quad (67)$$

The incident wave elevation is given by:

$$\zeta_I = a\,\exp\left[-i\,k_I\,(x\cos\beta\,-\,y\sin\beta)\right] \quad (68)$$

When evaluating diffraction potentials, it was found that a significant amount of time was often required for solving diffraction source strengths in Equation (63). The required solution time was noticeably greater than for the solution of radiation source strengths, which utilized hull symmetry. Both radiation and diffraction source strengths are solved using components of the linear algebra library LAPACK [15]. The computational time for solving a system of equations with LAPACK is approximately proportional to N^3, where N is the number of unknowns. To improve computational speed for evaluation of diffraction potentials, the incident wave potentials and corresponding diffraction potentials can be divided into components which are even and odd functions of y, thus taking advantage of ship symmetry. The even and odd components of the incident wave potential and their derivatives are:

$$\phi_I^{even} = \frac{i\,g\,a}{\omega_I}\,\exp(-i\,k_I\,x\,\cos\beta)\,\exp(k_I\,z_{wl})\,\cos(k_I\,y\,\sin\beta) \quad (69)$$

$$\frac{\partial \phi_I^{even}}{\partial x} = a\,\omega_I\,\cos\beta\,\exp(-i\,k_I\,x\,\cos\beta)\,\exp(k_I\,z_{wl})\,\cos(k_I\,y\,\sin\beta) \quad (70)$$

$$\frac{\partial \phi_I^{even}}{\partial y} = -a\,\omega_I\,\sin\beta\,\exp(-i\,k_I\,x\,\cos\beta)\,\exp(k_I\,z_{wl})\,\cos(k_I\,y\,\sin\beta) \quad (71)$$

$$\frac{\partial \phi_I^{even}}{\partial z} = i\,a\,\omega_I\,\exp\left(-i\,k_I\,x\cos\beta\right)\,\exp(k_I\,z_{wl})\,\cos(k_I\,y\,\sin\beta) \quad (72)$$

$$\phi_I^{odd} = \frac{i\,g\,a}{\omega_I}\,\exp(-i\,k_I\,x\,\cos\beta)\,\exp(k_I\,z_{wl})\,i\sin(k_I\,y\,\sin\beta) \quad (73)$$

$$\frac{\partial \phi_I^{odd}}{\partial x} = a\,\omega_I\,\cos\beta\,\exp(-i\,k_I\,x\,\cos\beta)\,\exp(k_I\,z_{wl})\,i\sin(k_I\,y\,\sin\beta) \quad (74)$$

$$\frac{\partial \phi_I^{odd}}{\partial y} = -a\,\omega_I\,\sin\beta\,\exp(-i\,k_I\,x\,\cos\beta)\,\exp(k_I\,z_{wl})\,i\sin(k_I\,y\,\sin\beta) \quad (75)$$

$$\frac{\partial \phi_I^{odd}}{\partial z} = i\,a\,\omega_I\,\exp\left(-i\,k_I\,x\cos\beta\right)\,i\sin(k_I\,y\,\sin\beta) \quad (76)$$

Using the even and odd components of incident wave potential, source strengths only have to be solved for the port side of the hull using the following:

$$[D^{even}]\,\{\sigma_D^{even}\} = \{-\partial\phi_I^{even}/\partial n\} \quad (77)$$

$$\left[D^{odd}\right]\,\left\{\sigma_D^{odd}\right\} = \left\{-\partial\phi_I^{odd}/\partial n\right\} \quad (78)$$

where $\{\sigma_D^{even}\}$ is the vector of source strengths on the port side for the even component of diffraction potential, $\{\partial\phi_I^{even}/\partial n\}$ is the vector of incident normal velocity on the port side due to the even component of the incident wave potential, $\left\{\sigma_D^{odd}\right\}$ is the vector of source strengths on the port side for the odd component of diffraction potential, and $\left\{\partial\phi_I^{odd}/\partial n\right\}$ is the vector of incident normal velocity on the port side due to the odd component of the incident wave potential. Once the source strengths are solved, the total diffracted potential on the hull can be determined by:

$$\left\{\begin{array}{c}\phi_D^{port}\\ \hline \phi_D^{star}\end{array}\right\} = \left[\begin{array}{c|c}E^{port,port} & E^{port,star}\\ \hline E^{port,star} & E^{port,port}\end{array}\right]\left\{\begin{array}{c}\sigma_D^{even}\\ \hline \sigma_D^{even}\end{array}\right\} + \left[\begin{array}{c|c}E^{port,port} & E^{port,star}\\ \hline E^{port,star} & E^{port,port}\end{array}\right]\left\{\begin{array}{c}\sigma_D^{odd}\\ \hline -\sigma_D^{odd}\end{array}\right\} \quad (79)$$

where $\left\{\phi_D^{port}\right\}$ is the vector of diffraction potentials on the port side of the hull, $\{\phi_D^{star}\}$ is the vector of diffraction potentials on the starboard side of the hull, $[E^{port,port}]$ is the influence matrix of velocity potentials on the port side due to sources on the port side, and $[E^{port,star}]$ is the influence matrix of velocity potentials on the port side due to sources on the starboard side.

The new procedure for evaluating diffraction source strengths requires approximately one quarter of the computation time as the original procedure. Although 2 sets of source strengths are now solved (even and odd), each set only has to be solved for half of the hull.

5.10 Interpolation of Inverse of Normal Velocity Influence Matrix when Evaluating Diffraction Potentials

The database of radiation and diffraction potentials previously mentioned allows rapid evaluation using interpolation of stored values. A comprehensive database encompassing full ranges of speeds, headings, and wave frequencies can require diffraction computations for several thousand sets of conditions. The previous subsection noted that diffraction potentials are evaluated using Equations (57), (58) and (79). When generating the database, the number of required Green function evaluations is greatly reduced using the following interpolation scheme presented in Reference 1:

$$\left[D^{port,port}(\omega_e)\right] = w_i\left[D^{port,port}(\omega_{e,i})\right] + w_{i+1}\left[D^{port,port}(\omega_{e,i+1})\right] \quad (80)$$

$$\left[D^{port,star}(\omega_e)\right] = w_i\left[D^{port,star}(\omega_{e,i})\right] + w_{i+1}\left[D^{port,star}(\omega_{e,i+1})\right] \quad (81)$$

$$\left[E^{port,port}(\omega_e)\right] = w_i\left[E^{port,port}(\omega_{e,i})\right] + w_{i+1}\left[E^{port,port}(\omega_{e,i+1})\right] \quad (82)$$

$$\left[E^{port,star}(\omega_e)\right] = w_i\left[E^{port,star}(\omega_{e,i})\right] + w_{i+1}\left[E^{port,star}(\omega_{e,i+1})\right] \quad (83)$$

where w_i and w_{i+1} are weights for linear interpolation and $\omega_{e,i} \leq \omega_e \leq \omega_{e,i+1}$. When using the above interpolation scheme, a large amount of computational time can still be required because the diffraction source strengths must still be solved (solution of σ_D^{even} and σ_D^{odd} that satisfy Equations (57) and (58)) for each combination of ship speed, heading, and wave frequency. This solution time can be greatly reduced by interpolation of the inverse of $[D^{even}]$ and $[D^{odd}]$ as follows:

$$[D^{even}(\omega_e)]^{-1} = w_i \; [D^{even}(\omega_{e,i})]^{-1} + w_{i+1} \; [D^{even}(\omega_{e,i+1})]^{-1} \quad (84)$$

$$\left[D^{odd}(\omega_e)\right]^{-1} = w_i \; \left[D^{odd}(\omega_{e,i})\right]^{-1} + w_{i+1} \; \left[D^{odd}(\omega_{e,i+1})\right]^{-1} \quad (85)$$

Using the interpolated inverses, the source strengths are then quickly evaluated using:

$$\{\sigma_D^{even}\} = [D^{even}(\omega_e)]^{-1} \{-\partial\phi_I^{even}/\partial n\} \quad (86)$$

$$\left\{\sigma_D^{odd}\right\} = \left[D^{odd}(\omega_e)\right]^{-1} \left\{-\partial\phi_I^{odd}/\partial n\right\} \quad (87)$$

The potential benefits of the above interpolation scheme become obvious when one considers that a representative database of diffraction forces could include 7 ship speeds (0, 5, . . ., 30 knots), 13 sea directions (0, 15, . . ., 180 degrees), and 37 wave frequencies (0.20, 0.25, . . ., 2.00 rad/s), giving a total of 3367 seaway conditions. The same database could have 60 encounter frequencies (0.1, 0.2, . . ., 6.0 rad/s).

It should be noted that there is loss of accuracy when interpolating influence matrices using Equations (80) to (83). The interpolation of inverse matrices using Equations (84) and (85) likely leads to additional loss of accuracy. Losses in accuracy will likely be greatest in the vicinity of irregular frequencies of encounter, at which solved potentials can be sensitive to small variations in influence matrix terms.

5.11 New Procedure for Computation of Diffraction Forces from a Database

When predicting wave diffraction forces using previously computed values, the procedure presented in Reference 1 uses interpolation to obtain wave diffraction force in unit amplitude waves as a function of ship speed, heading, and wave frequency. The main disadvantage of this approach is that it does not adequately model the strong influence of wave encounter frequency on wave diffraction force. To obtain more accurate results, wave diffraction forces are now evaluated as follows:

$$F_j^D = a \left(\frac{\omega_e \; F_j^{D,\omega_e}}{a} + \frac{U \; F_j^{D,U}}{a} \right) \quad (88)$$

where F_j^{D,ω_e} is the diffraction force component that is proportional to wave encounter frequency and $F_j^{D,U}$ is the diffraction force component that is proportional to ship speed. Reference 1 gives the following equation for diffraction forces:

$$F_j^D = \rho\,\omega_e \int_{S_b} \left(i\phi_D - \frac{U}{\omega_e}\,\frac{\partial \phi_D}{\partial x} \right) n_j\, dS \tag{89}$$

where ϕ_D is the potential of the diffracted waves. The corresponding components for Equation (88) are:

$$F_j^{D,\omega_e} = \rho \int_{S_b} i\,\phi_D\, n_j\, dS \tag{90}$$

$$F_j^{D,U} = -\,\rho \int_{S_b} \frac{\partial \phi_D}{\partial x}\, n_j\, dS \tag{91}$$

When creating a database of hull radiation and diffraction forces, each of the above components in unit amplitude waves are stored for combinations of specified ship speeds, headings, and wave frequencies. When accessing values from the database, the above components are interpolated as functions of ship speed, heading, and wave frequency.

5.12 Faster Versions of LAPACK Routines for Solution of Systems of Linear Equations

When solving radiation and diffraction potentials, a large amount of CPU time is devoted to solving systems of linear equations. Routines from the LAPACK library [15] are used for solving systems linear equations. Previously, functions *solve_linear_equations* and *inverse* from the Python Numeric library [16] were used for solving linear equations and inverting matrices. The Python package SciPy, available at no cost from http://www.scipy.org, has versions of LAPACK routines optimized for PC hardware. The SciPy routines *solve* and *inv* are now used instead of the Numeric routines *solve_linear_equations* and *inverse*.

Table 3 gives representative CPU times for solving hull added mass and damping coefficients in the frequency domain for HALIFAX. The values in Table 3 are based on average CPU times over a range of encounter frequencies. As expected, the amount of CPU time for solution of Green functions is approximately proportional to $(N_p^{port})^2$. The CPU time required for matrix inversion or solution of equations without matrix inversion is approximately proportional to $(N_p^{port})^3$, which is also expected. The optimized inversion and solution routines from SciPy are approximately three times faster than the corresponding routines from Numeric. Solution of velocities using matrix inversion takes approximately three times longer than solution without matrix inversion; however, matrix inversion can be useful for determining matrix condition numbers, as discussed in Section 5.7.

Table 3: *Typical CPU Times (seconds) Per Encounter Frequency for Prediction of Hull Added Mass and Damping Coefficients in Frequency Domain*

	Coarse mesh N_p^{port} = 224	Medium mesh N_p^{port} = 433	Fine mesh N_p^{port} = 1040
Evaluation of Green functions and derivatives	30	110	637
Inversion of influence matrices for even and odd modes using Numeric routine *inverse*	2.1	17	250
Inversion of influence matrices for even and odd modes using SciPy routine *inv*	0.47	2.9	45
Solution of velocity potentials for even and odd modes using Numeric routine *solve_linear_equations*	0.46	4.8	81
Solution of velocity potentials for even and odd modes using SciPy routine *solve*	0.16	1.0	15

6 Hydrodynamic Forces in the Frequency Domain for HALIFAX

To verify the improved methods presented in the previous section, hydrodynamic forces in the frequency domain have been computed for HALIFAX. The coarse, medium, and fine meshes presented in Section 4 have been used. Table 4 gives parameters for generated databases of ship hydrodynamic coefficients in the frequency domain. To suppress irregular frequency effects, limiting envelopes on matrix condition numbers were provided as input. These envelopes are shown in Figures 13 and 14, and were developed by examining initial predictions of hydrodynamic coefficients and matrix condition numbers presented in Figure 7 to 12

Table 4: *Parameters for Databases of Frequency Domain Radiation and Diffraction Forces*

Wave encounter frequencies ω_e	0.1, 0.2, 0.3, . . ., 6.0 rad/s
Ship speeds U	0, 5, 10, 15, 20, 25, 30 knots
Relative sea directions β	30, 150, 165, 180 degrees
Wave frequencies ω_I	0.20, 0.25, 0.30, . . ., 2.0 rad/s

Table 5 gives required computation times for generating the databases of hydrodynamic forces in the frequency domain. As discussed in Section 5, wave diffraction computations can be performed more quickly but somewhat less accurately using interpolation of influence matrix inverses according to Equations (84) and (85). The computational times given in Table 5 are based on the more accurate approach of interpolation of influence matrices rather than their inverses.

Table 5: *Required CPU Time for Generating Database of Radiation and Diffraction Computations*

Mesh	CPU time
Coarse, N_p^{port} = 224	0.7 hours
Medium, N_p^{port} = 433	2.6 hours
Fine, N_p^{port} = 1040	16.8 hours

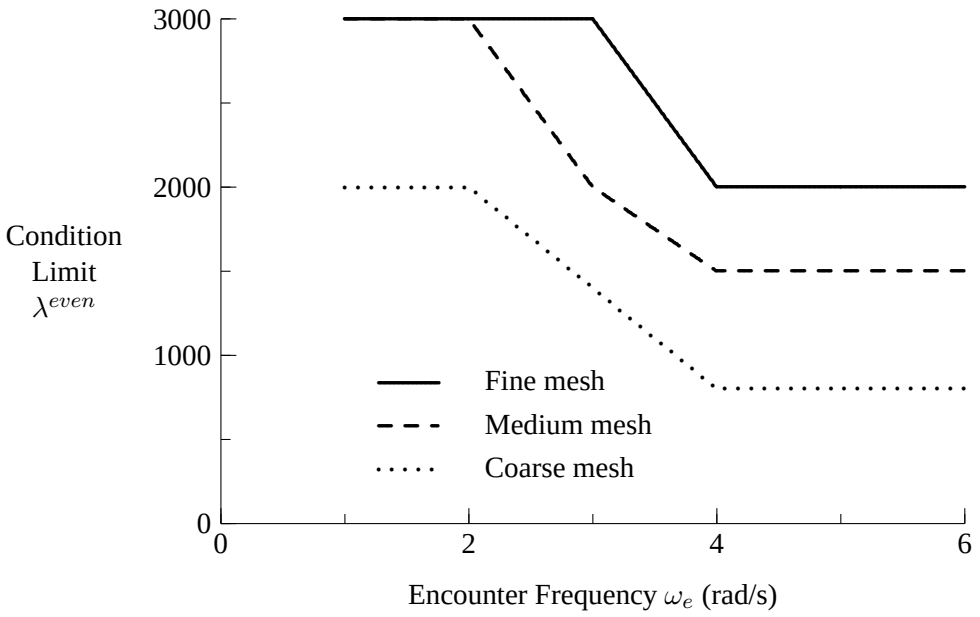

Figure 13: *HALIFAX Limiting Condition Numbers for Longitudinal Modes Surge, Heave, and Pitch*

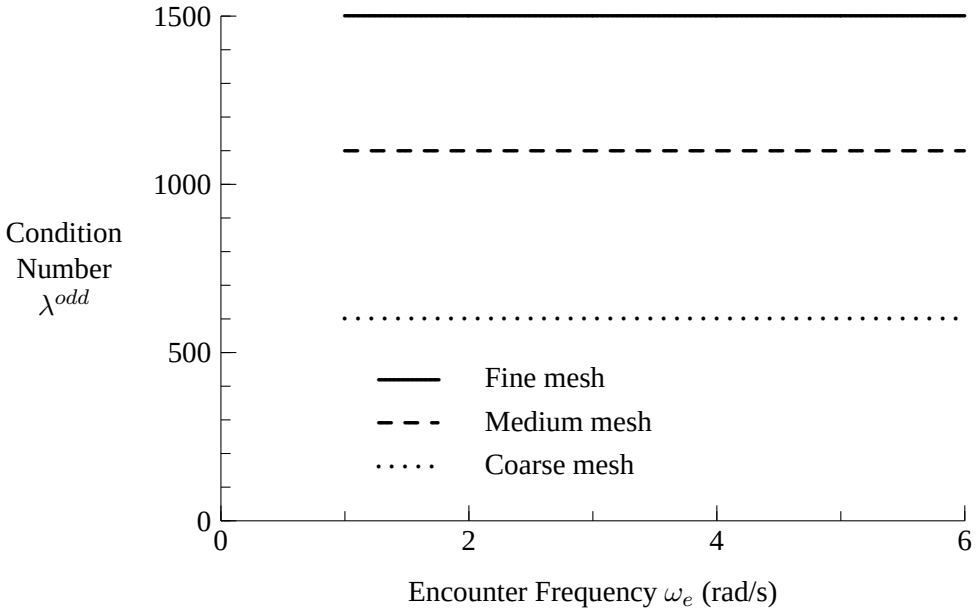

Figure 14: *HALIFAX Limiting Condition Numbers for Lateral Modes Sway, Roll, and Yaw*

6.1 Damping and x Derivative of Added Mass

Figures 15 to 20 show damping and the x derivative of added mass for HALIFAX. These two quantities are shown because they are both used for determining retardation functions in the time domain. The plots of damping and x derivative of added mass have been non-dimensionalized to indicate their relative magnitudes for a ship speed of 20 knots. This speed was selected because it is approaching the maximum speed at which HALIFAX would typically transit in a moderate to heavy seaway. Damping coefficients from the 3 different meshes have very similar values. The x derivatives of added mass are more sensitive to mesh size because they are small quantities arising from fore-aft asymmetry of the ship hull. The good agreement between the medium and fine meshes indicates numerical convergence with increasing number of panels.

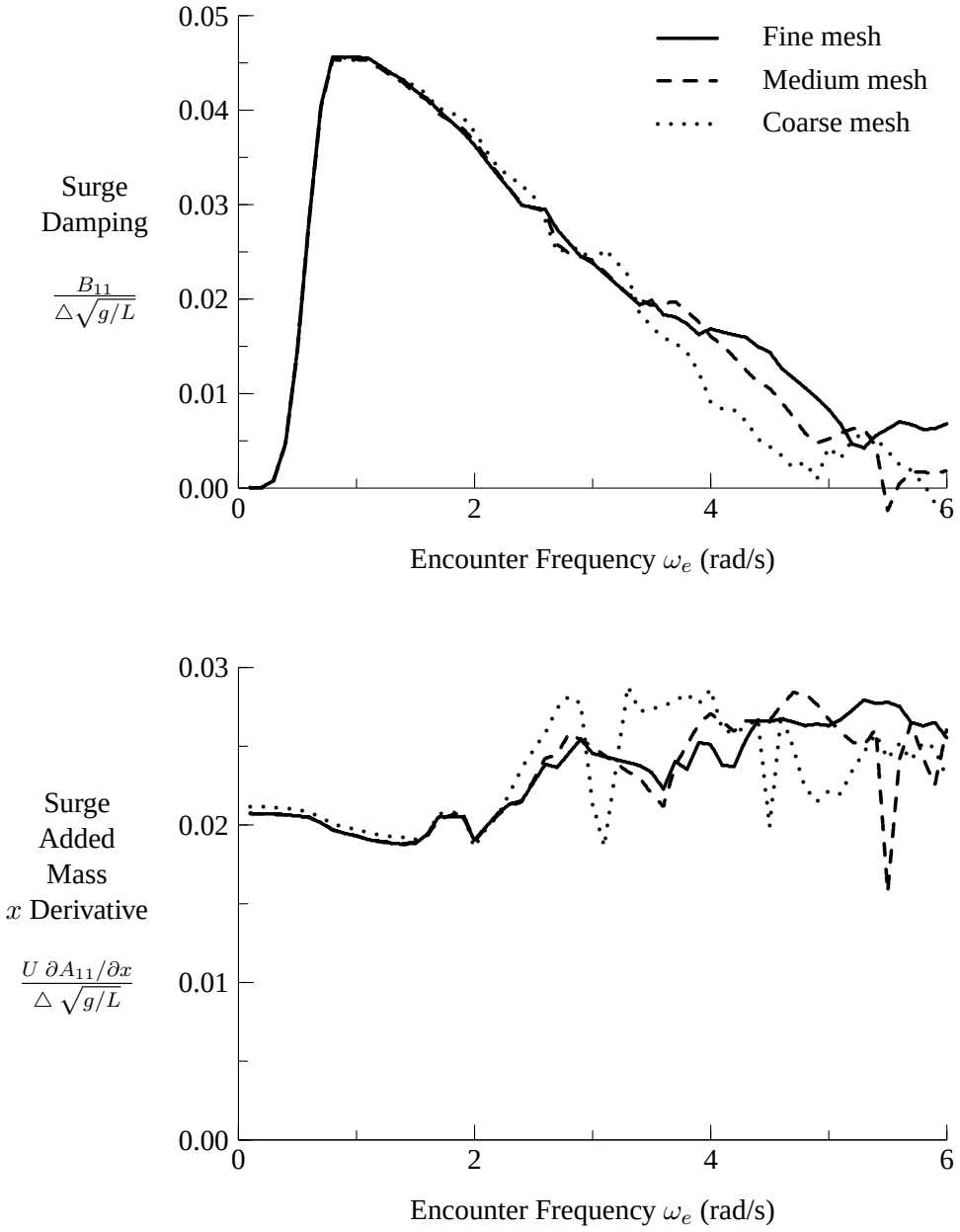

Figure 15: *Dimensionless Forces from Zero Speed Surge Damping and x Derivative of Added Mass for HALIFAX at 20 Knots*

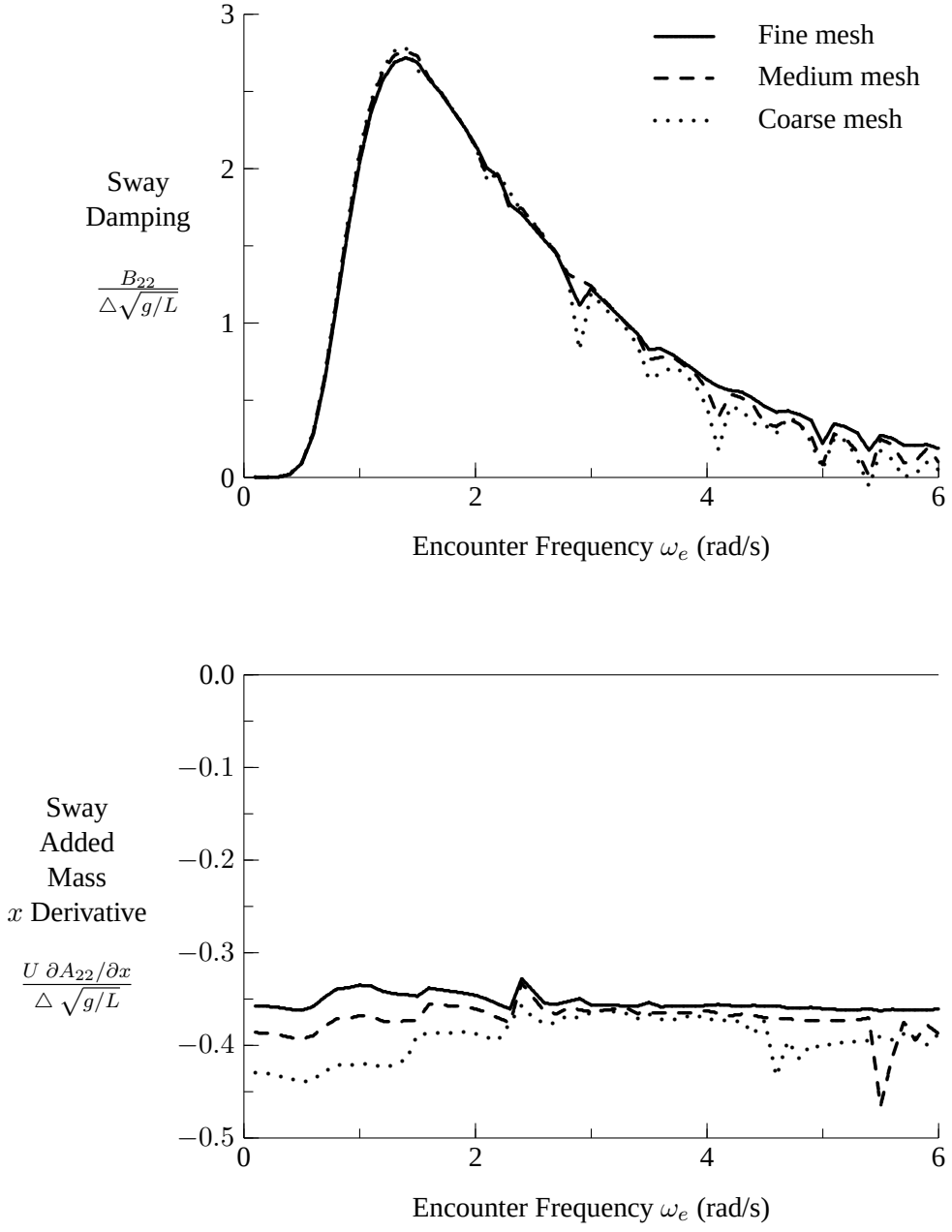

Figure 16: *Dimensionless Forces from Zero Speed Sway Damping and x Derivative of Added Mass for HALIFAX at 20 Knots*

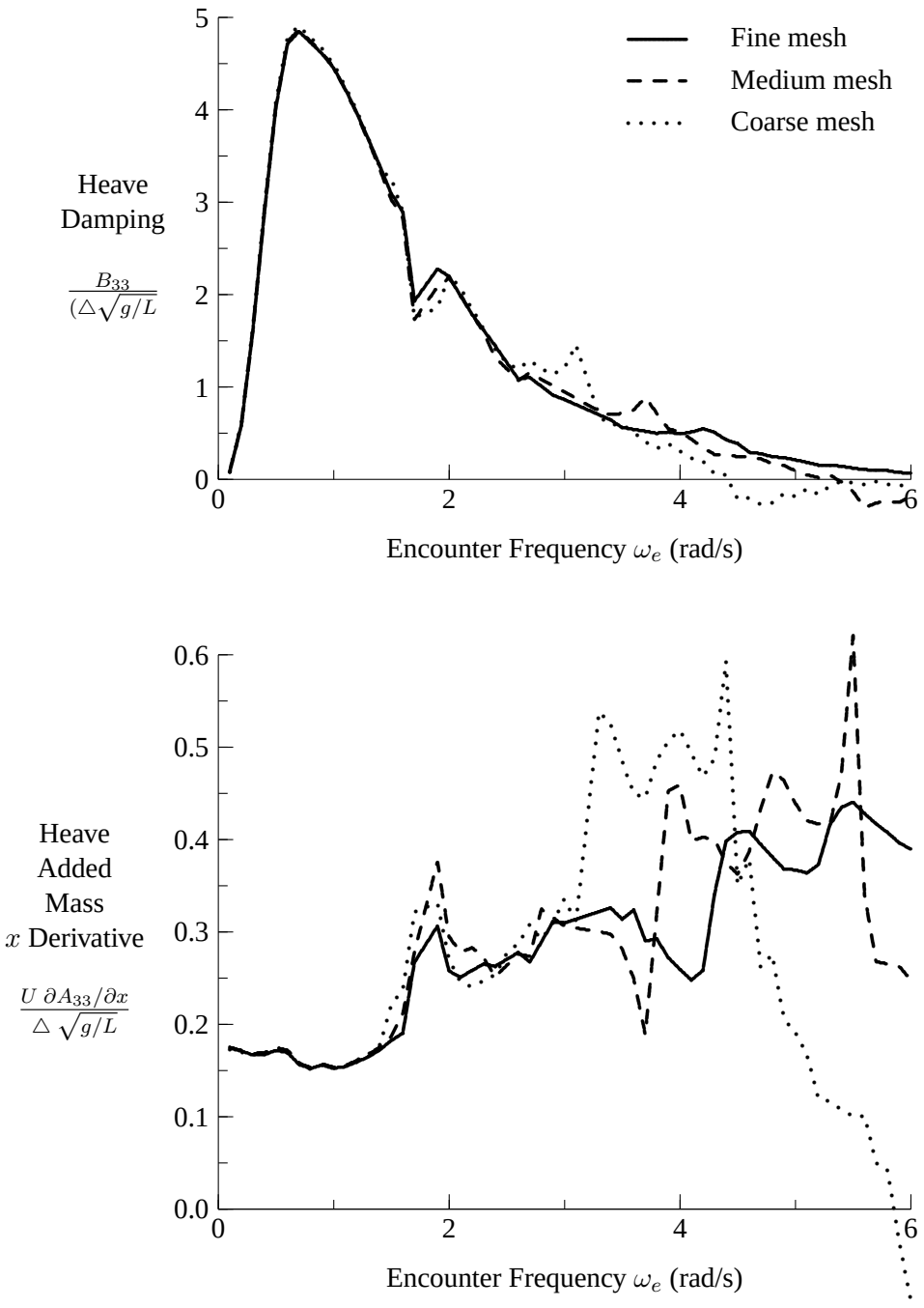

Figure 17: *Dimensionless Forces from Zero Speed Heave Damping and x Derivative of Added Mass for HALIFAX at 20 Knots*

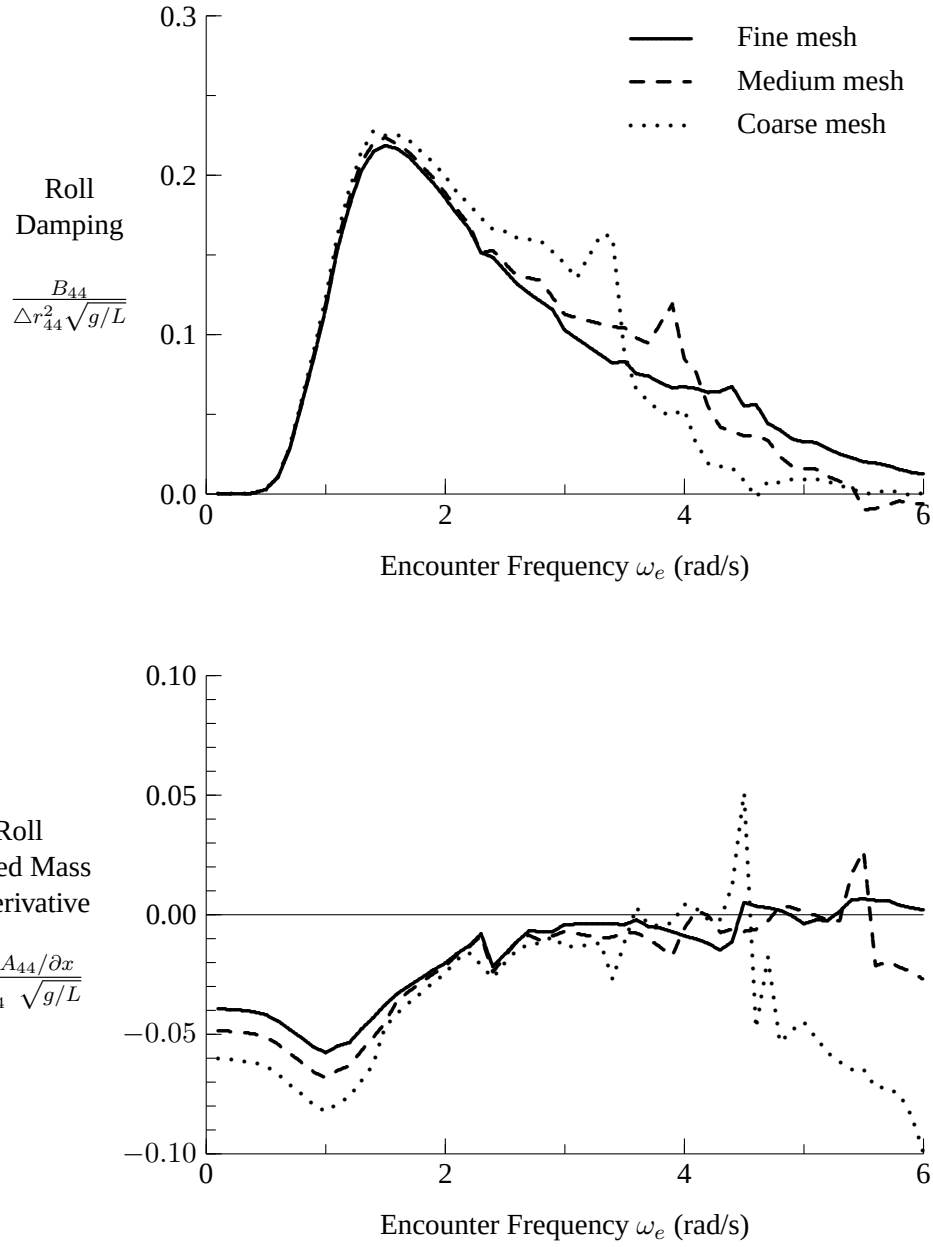

Figure 18: *Dimensionless Forces from Zero Speed Roll Damping and x Derivative of Added Mass for HALIFAX at 20 Knots*

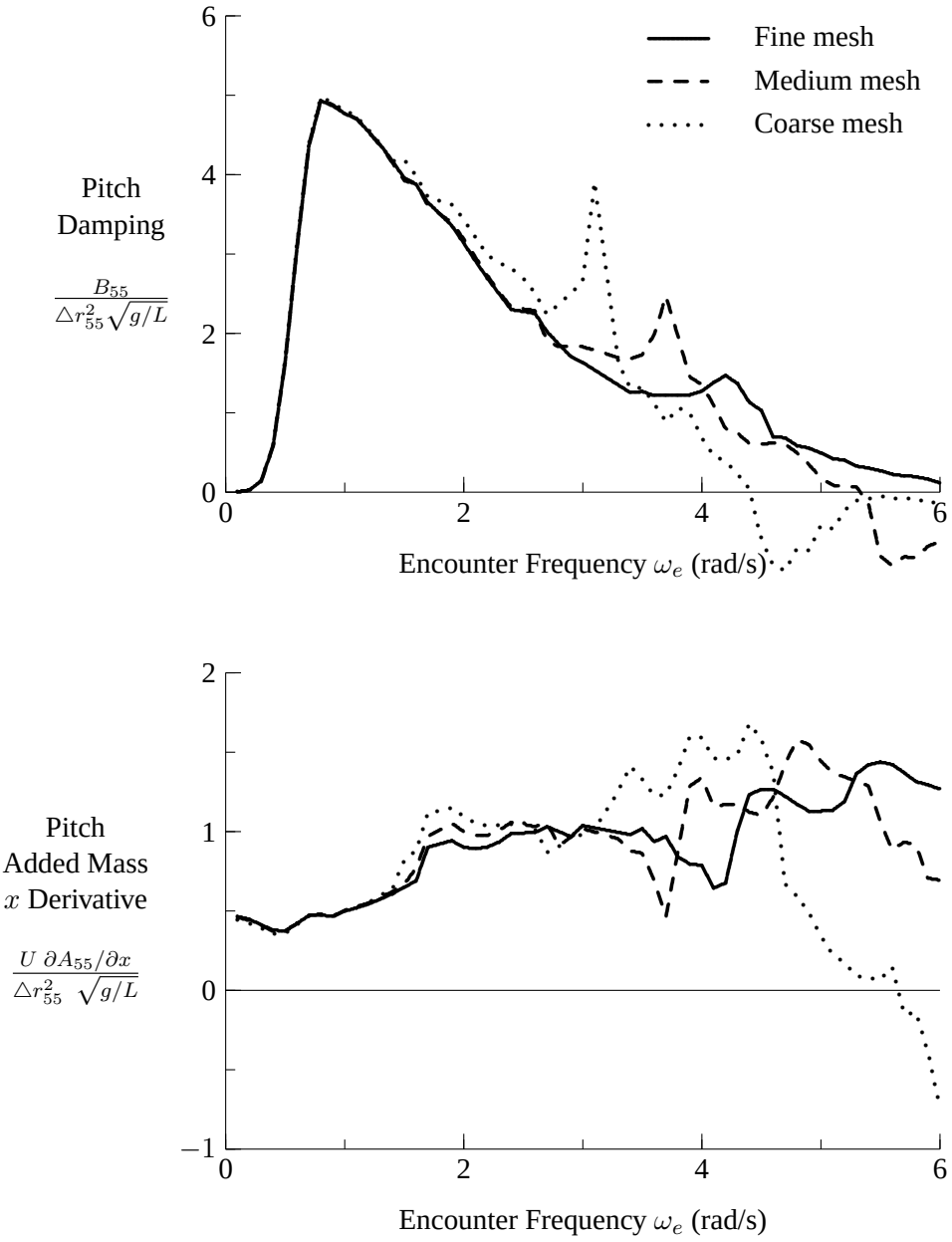

Figure 19: *Dimensionless Forces from Zero Speed Pitch Damping and x Derivative of Added Mass for HALIFAX at 20 Knots*

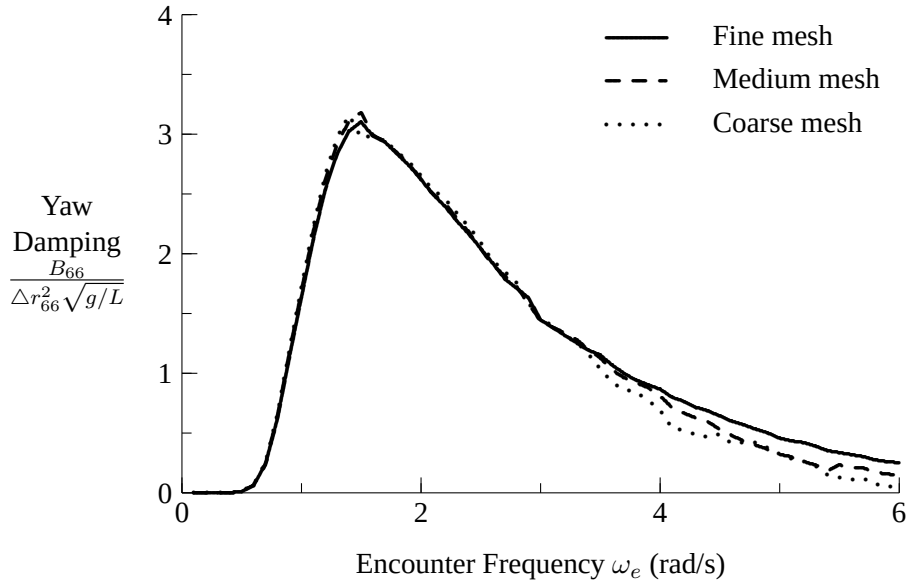

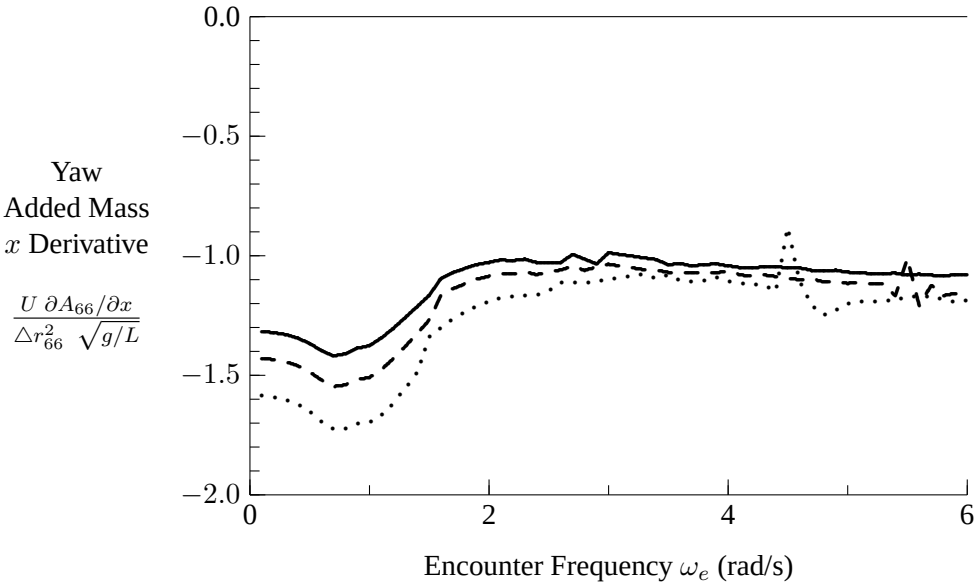

Figure 20: *Dimensionless Forces from Zero Speed Yaw Damping and x Derivative of Added Mass for HALIFAX at 20 Knots*

6.2 Wave Excitation Forces on HALIFAX

Figures 21 and 22 show wave excitation forces on HALIFAX for a ship speed of 20 knots in stern quartering and bow quartering seas. All results are for the medium mesh using the following three computational methods, listing in order of decreasing computational time:

- normal velocity influence matrix $[D(\omega_e)]$ computed directly at frequency ω_e,
- normal velocity influence matrix $[D(\omega_e)]$ obtained using interpolation from adjacent encounter frequencies in database (Equations (80) and (81)),
- inverse of normal velocity influence matrix $[D(\omega_e)]^{-1}$ obtained using interpolation from adjacent encounter frequencies in database (Equations (84) and (85)).

For the most part, the three approaches give excellent agreement. Discrepancies are limited to when the matrix $[D(\omega_e)]^{-1}$ is interpolated for bow quartering seas with wave frequencies in the vicinity of 1.0-1.2 rad/s. The associated encounter frequencies are of the order 2-3 rad/s, where the first irregular frequencies occur for longitudinal and lateral modes, and small errors in influence matrix terms can lead to large errors in computed solutions. In summary, the above results indicate that reliable diffraction forces can be obtained when interpolating the influence matrix $[D]$ as a function of encounter frequency. If the inverse matrix $[D]^{-1}$ is interpolated as a function of encounter frequency, noticeable inaccuracies can occur in the vicinity of irregular frequencies.

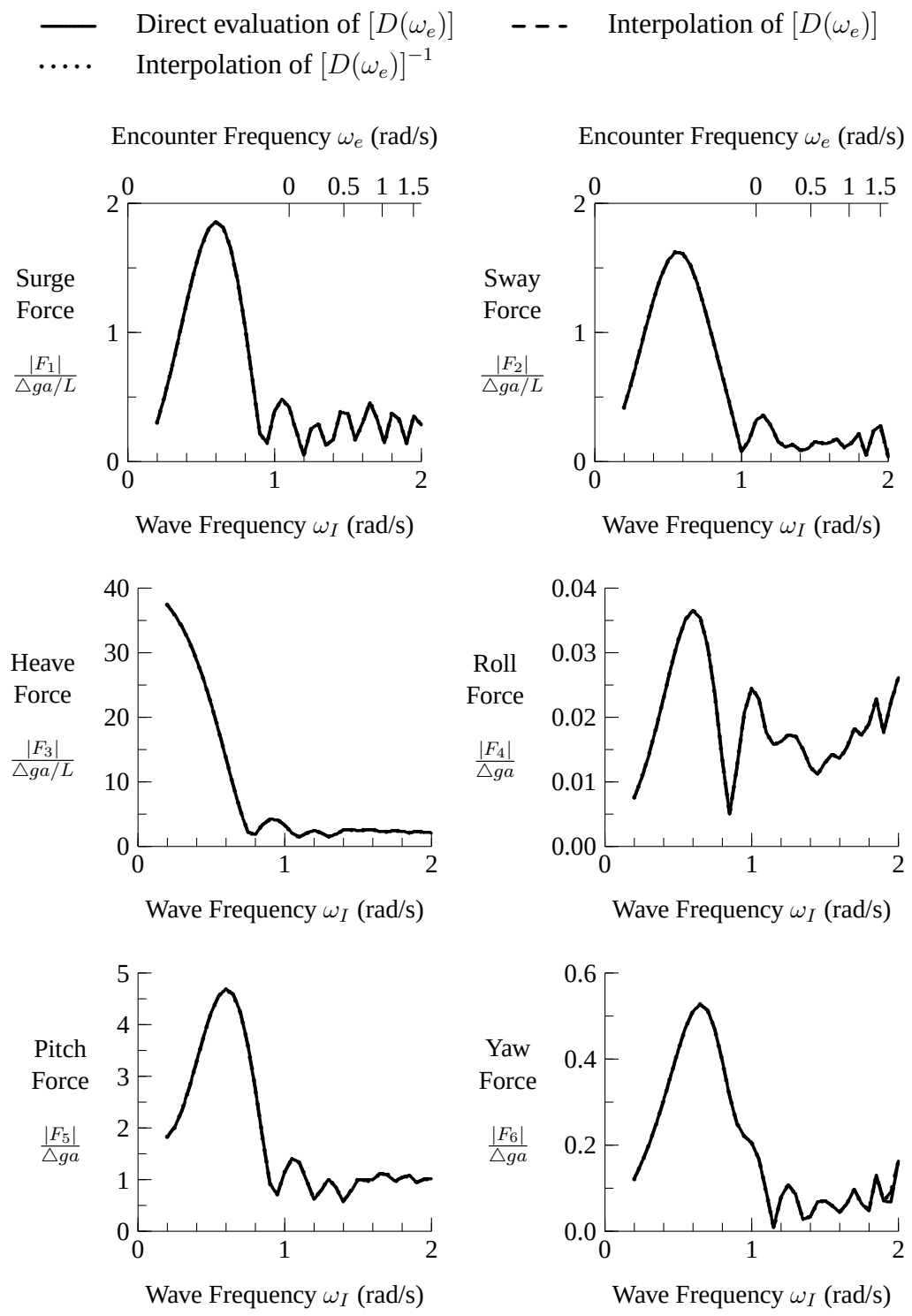

Figure 21: *Wave Excitation Forces for HALIFAX, Medium Mesh, 20 knots, Stern Quartering Seas at 30 degrees*

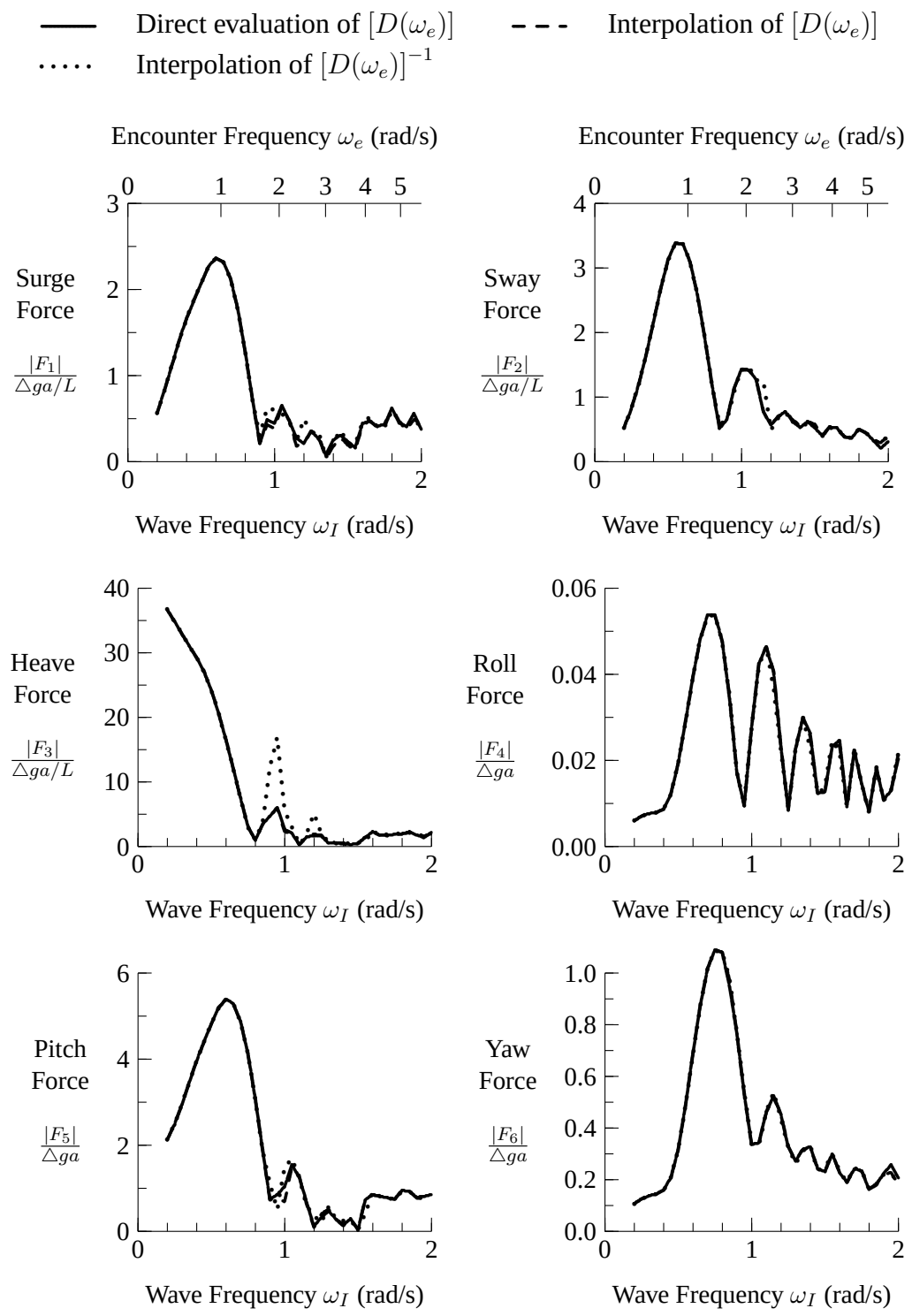

Figure 22: *Wave Excitation Forces for HALIFAX, Medium Mesh, 20 knots, Bow Quartering Seas at 150 degrees*

6.3 HALIFAX Motions in the Frequency Domain Using New Computational Methods

Motions for HALIFAX in stern quartering and bow quartering seas are presented in Figures 23 and 24. The motions based on directly computed hydrodynamic coefficients agree very closely with those from the database with interpolation of influence matrix $[D]$ as a function of encounter frequency. As was observed for wave excitation forces, some discrepancies occur in the vicinity of irregular frequencies when the inverse matrix $[D]^{-1}$ is interpolated as a function of encounter frequency. When high accuracy is required from a database of diffraction forces, the results indicate that one should interpolate the influence matrix $[D]$ rather than its inverse $[D]^{-1}$ as a function of encounter frequency

For the motions in stern quartering seas in Figure 23, wave frequencies have been excluded that have encounter frequencies less than 0.1 rad/s. At wave frequencies with encounter frequencies below 0.1 rad/s, predicted motions in unrestrained modes (surge, sway, and yaw) are unrealistically large due to the absence of restraining forces and very small inertia and damping forces. For practical computations, this problem can be avoided by a slight shift of wave frequency or by including viscous damping terms.

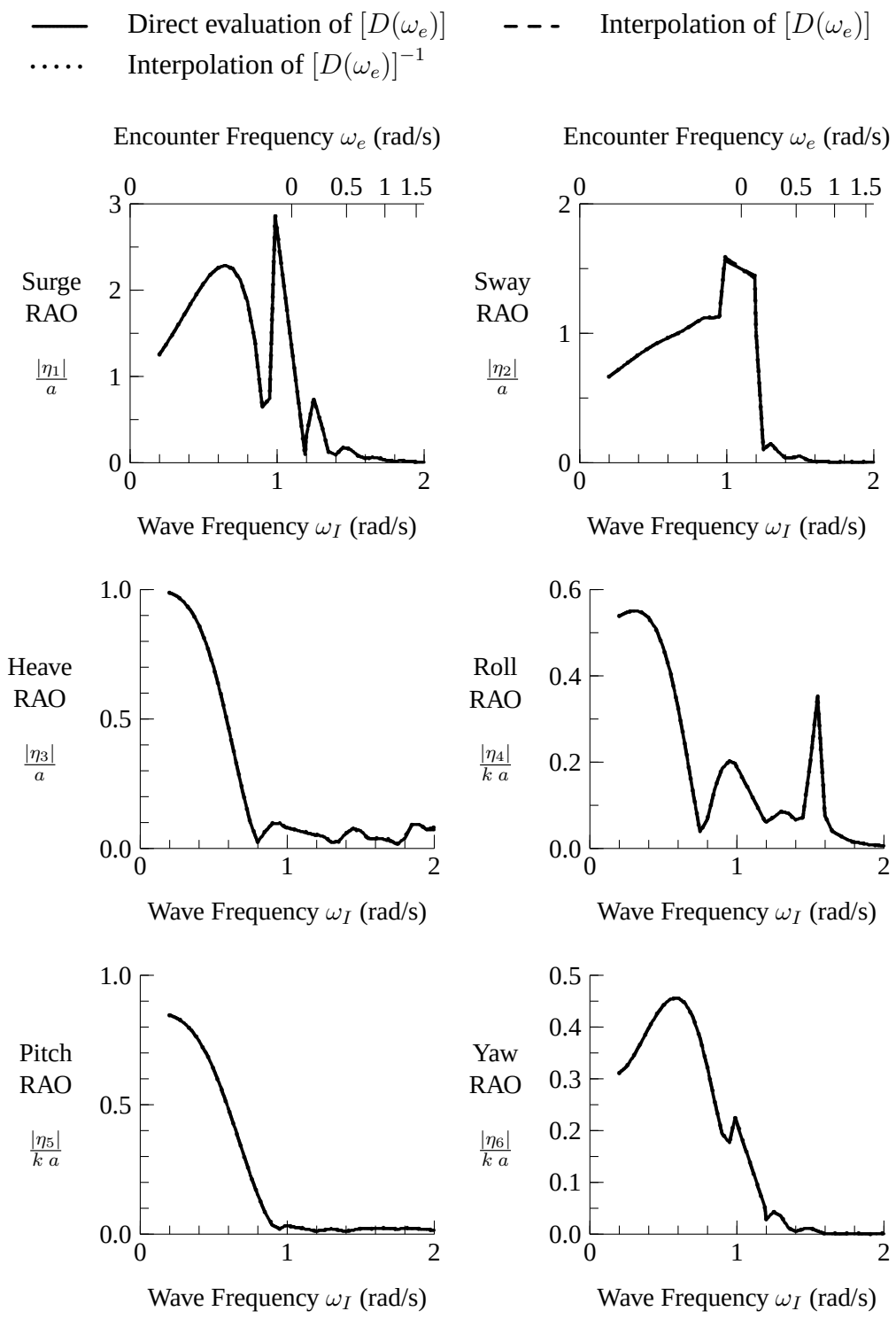

Figure 23: *Frequency Domain Motions for HALIFAX from Direct and Database Computations, Medium Mesh, 20 knots, Stern Quartering Seas at 30 degrees*

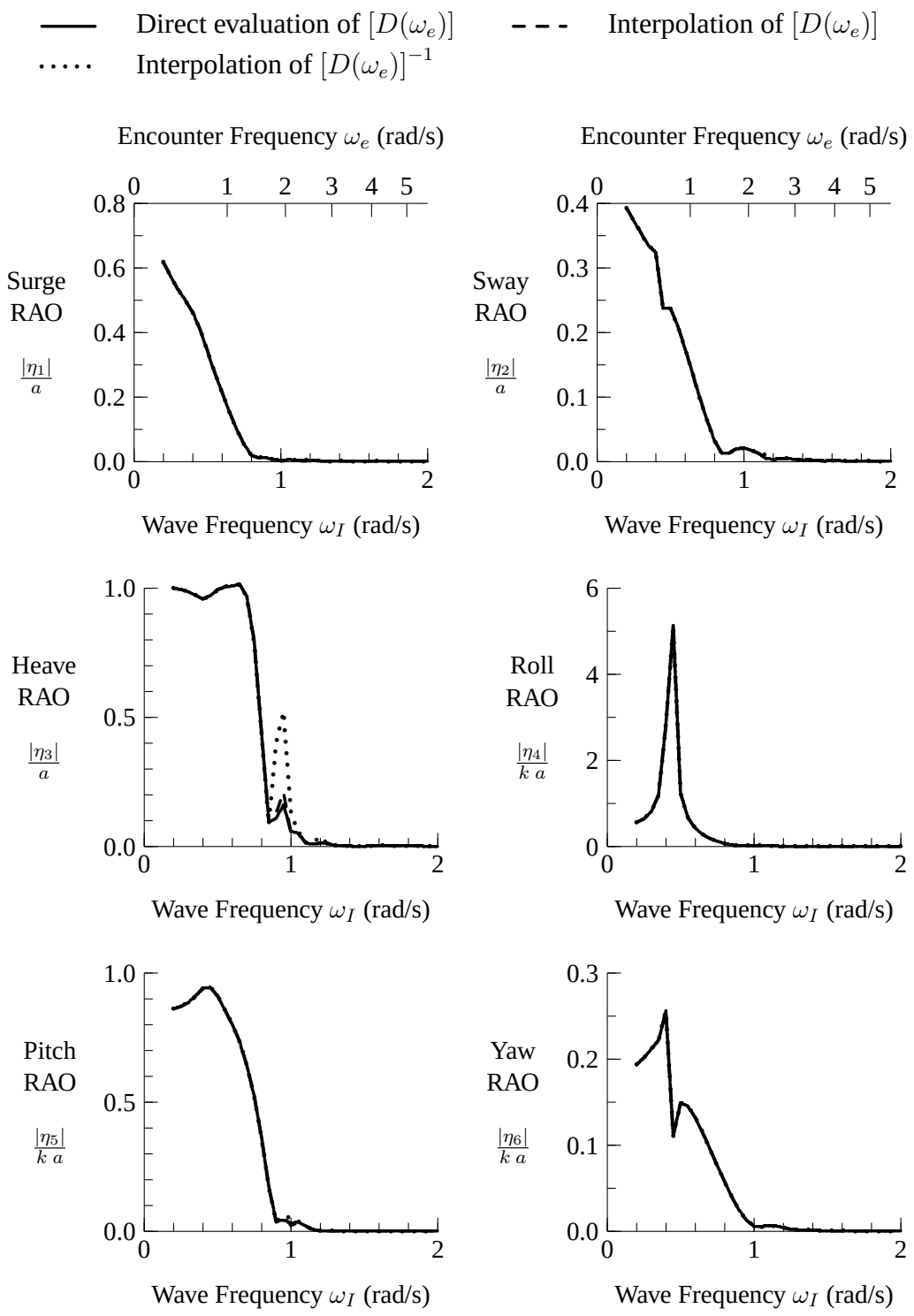

Figure 24: *Frequency Domain Motions for HALIFAX from Direct and Database Computations, Medium Mesh, 20 knots, Bow Quartering Seas at 150 degrees*

7 Hydrodynamic Coefficients in the Time Domain for HALIFAX

Retardation functions presented in Section 3 have been computed for HALIFAX using the frequency domain coefficients presented in the previous section. The computed retardation functions are based on numerical integration of frequency domain coefficients for an encounter frequency range of 0 to 6 rad/s with an increment of 0.05 rad/s. At encounter frequencies beyond 6 rad/s, damping and the x derivative of added mass are assumed to be equal to their infinite frequency values. Figures 25 to 30 show the resulting speed-independent and speed-dependent terms of retardation functions. As was done for frequency domain coefficients in Section 6, speed-dependent terms are given for a ship speed of 20 knots to indicate their magnitude relative to speed-independent terms.

Figures 25 to 30 show that the speed-independent terms are much greater than the speed-dependent terms for HALIFAX travelling at 20 knots. Similar behaviour was observed for frequency domain coefficients in Section 6. The medium and fine meshes give similar results; however, the coarse mesh gives significant differences in speed-dependent terms. These differences can be attributed to the relatively small magnitude of speed-dependent terms and their sensitivity to computed x derivatives of velocity potentials.

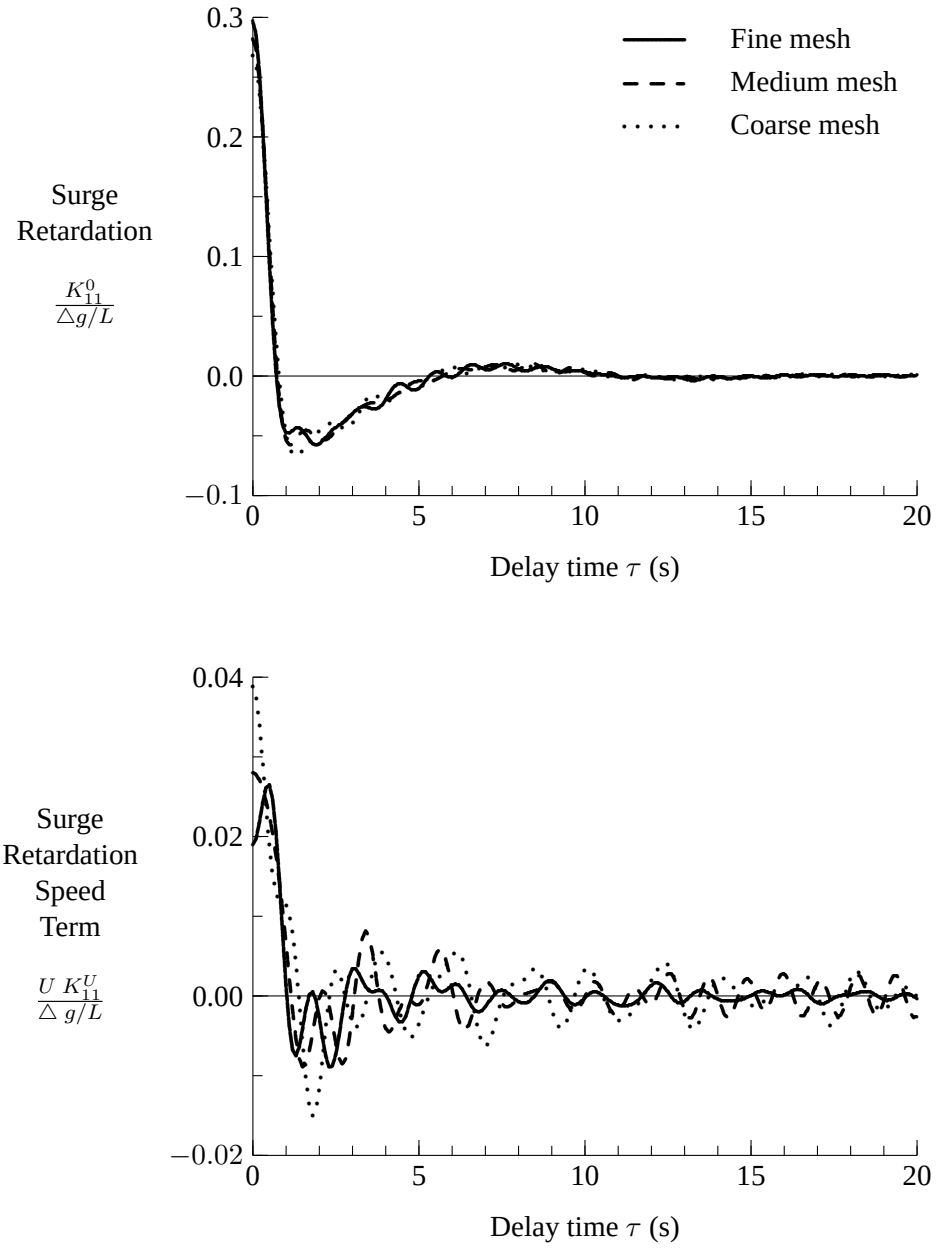

Figure 25: *HALIFAX Surge Retardation Contributions K_{11}^0 and UK_{11}^U for U = 20 knots*

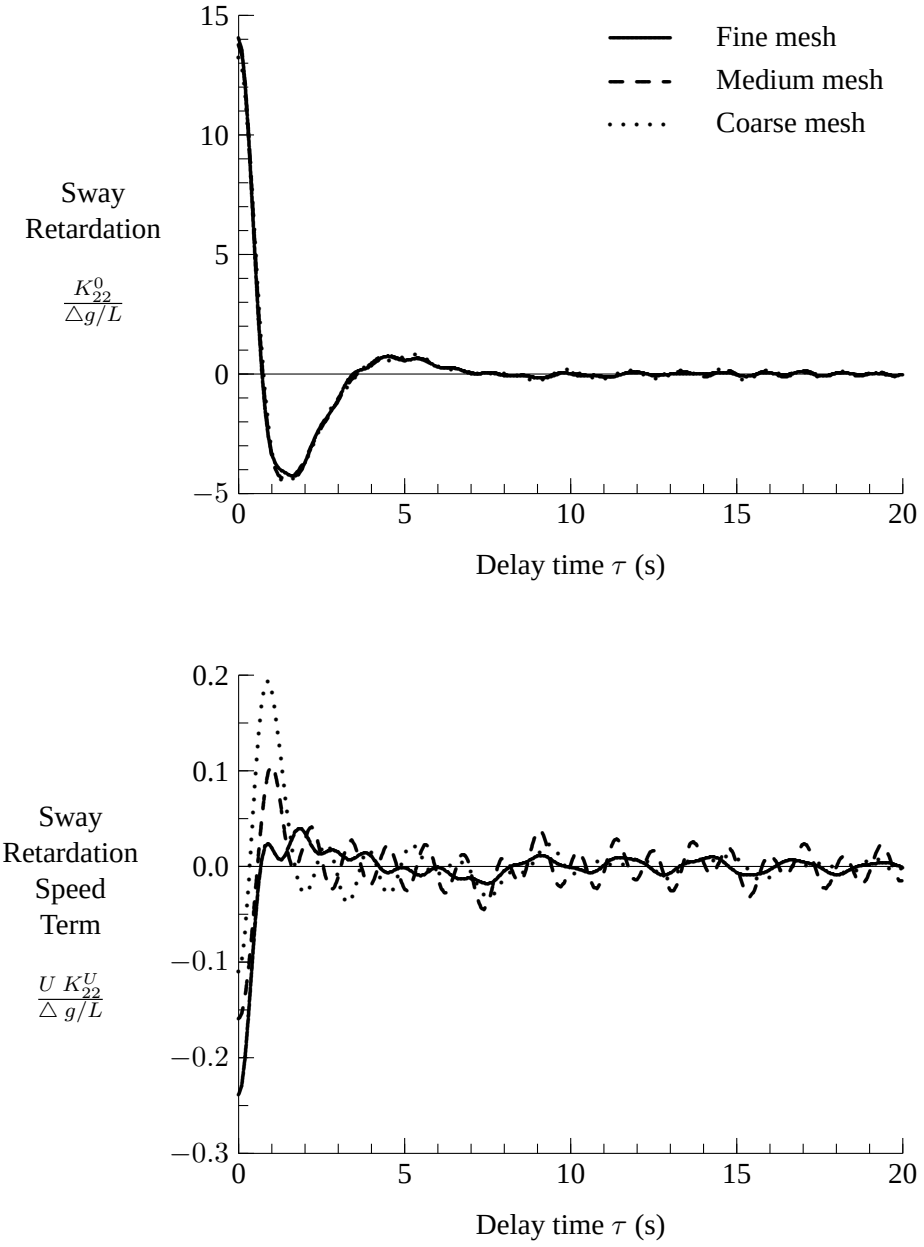

Figure 26: *HALIFAX Sway Retardation Contributions K_{22}^0 and UK_{22}^U for U = 20 knots*

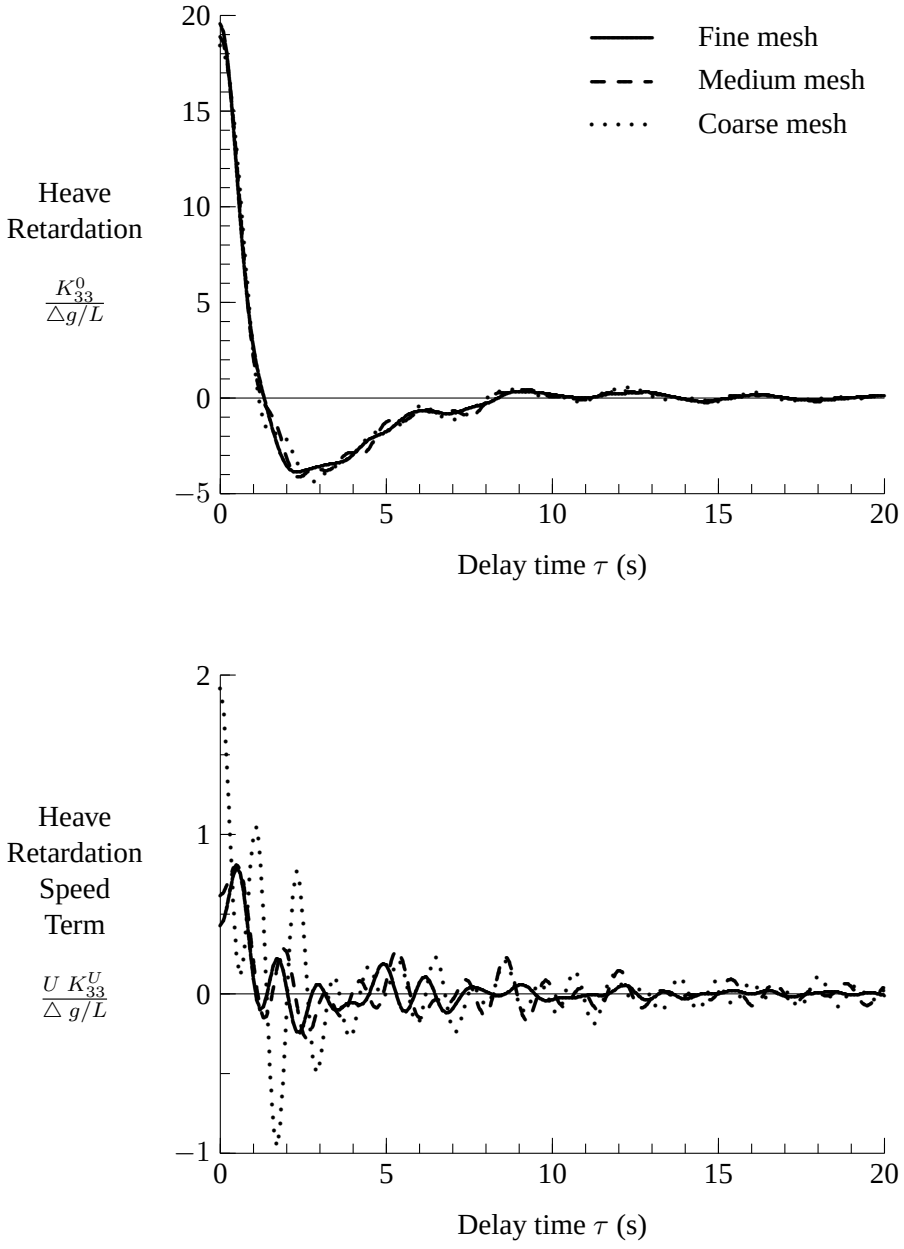

Figure 27: *HALIFAX Heave Retardation Contributions K_{33}^0 and UK_{33}^U for U = 20 knots*

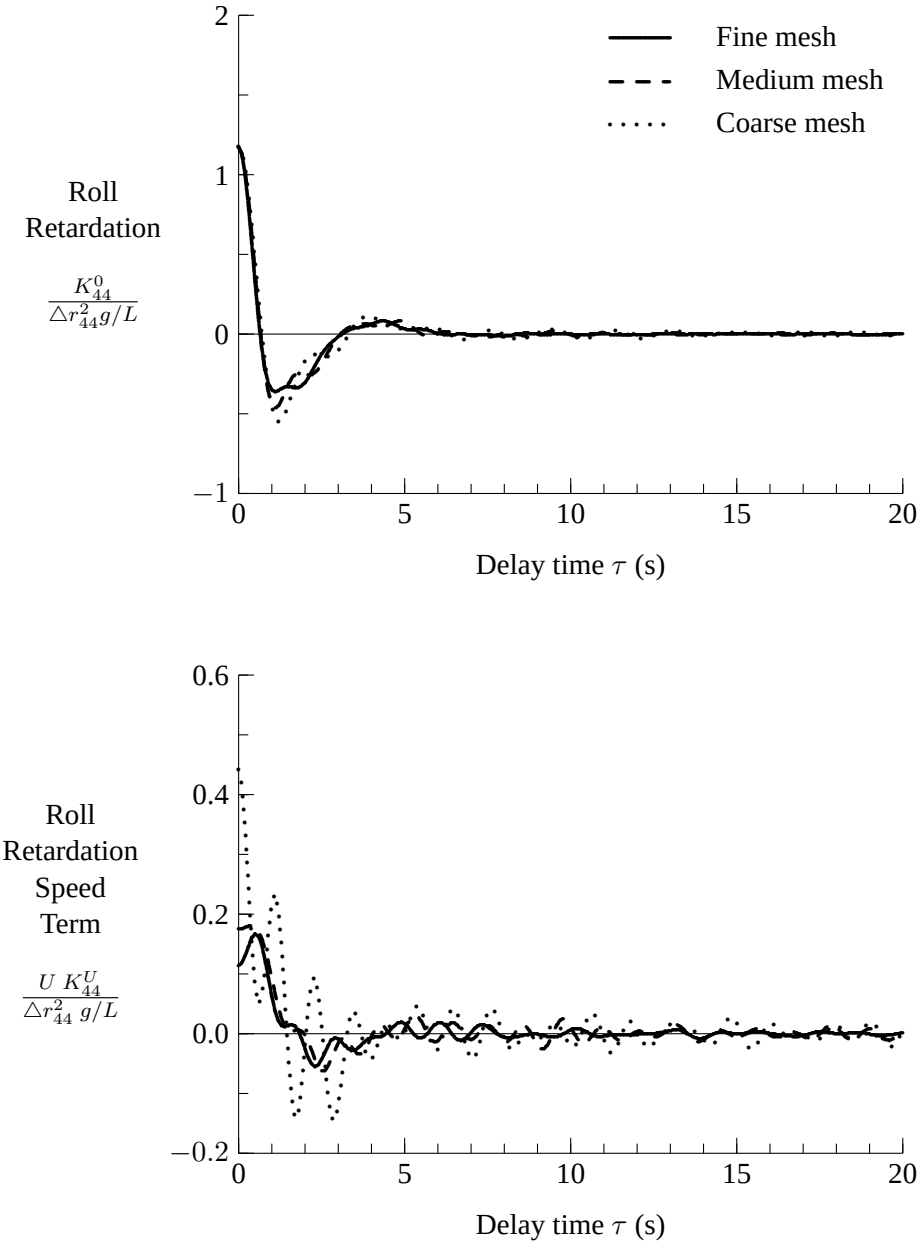

Figure 28: *HALIFAX Roll Retardation Contributions K_{44}^0 and UK_{44}^U for U = 20 knots*

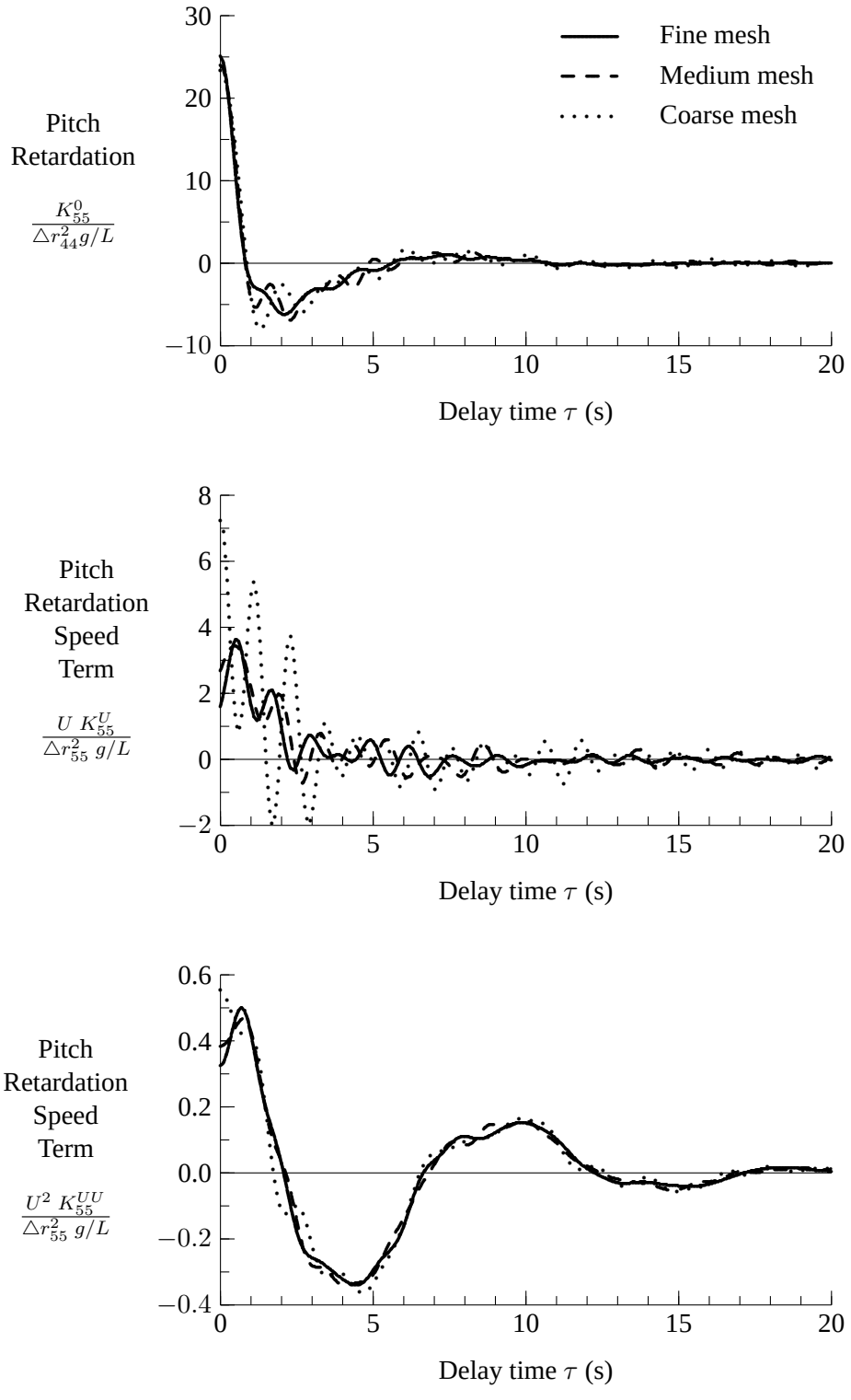

Figure 29: *HALIFAX Pitch Retardation Contributions K^0_{55}, UK^U_{55}, and $U^2K^{UU}_{55}$ for U = 20 knots*

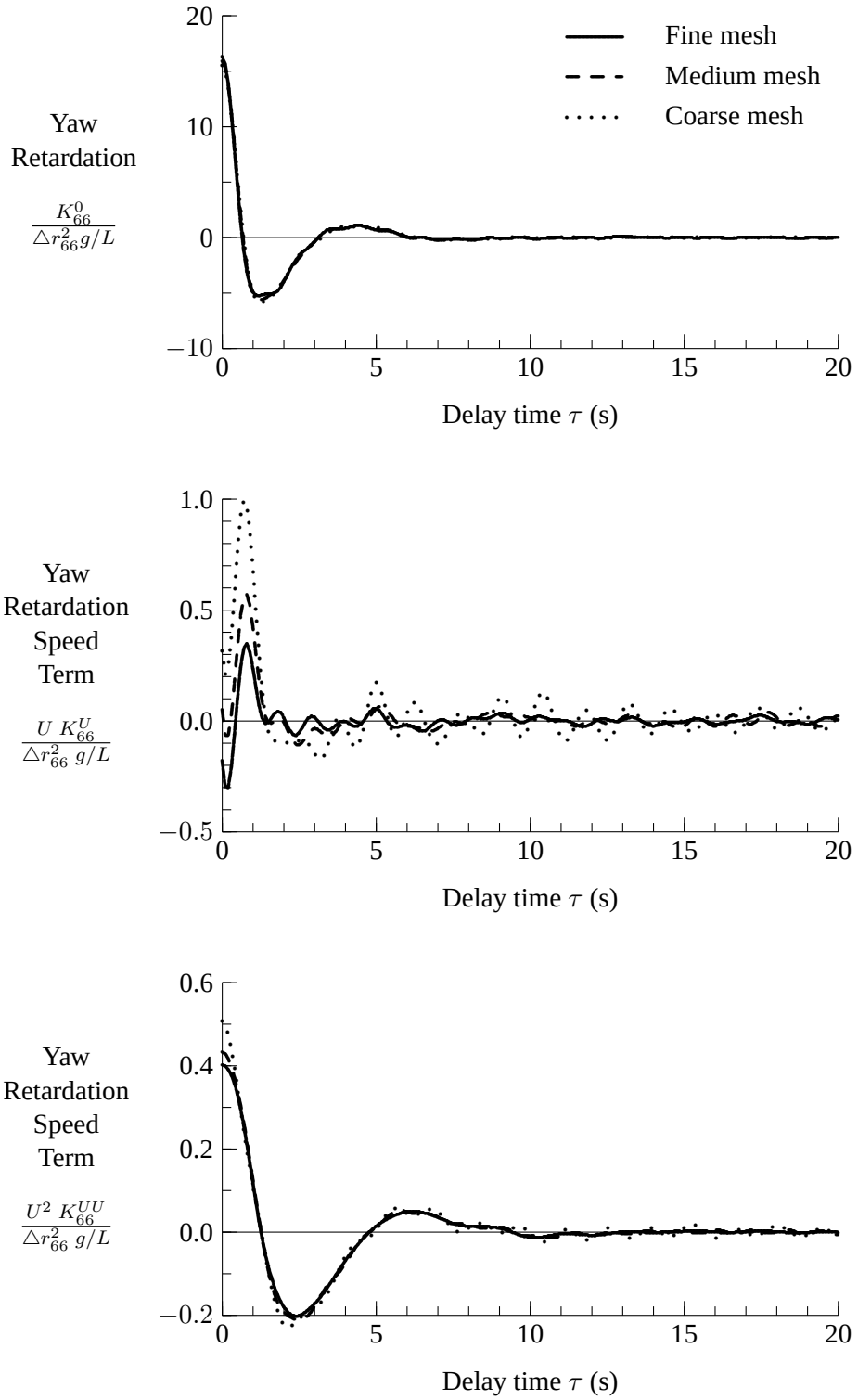

Figure 30: *HALIFAX Yaw Retardation Contributions K_{66}^0, UK_{66}^U, and $U^2K_{66}^{UU}$ for U = 20 knots*

8 Time Domain Simulation of Ship Motions

The hydrodynamic forces presented in this report can form the basis for simulating motions of an unappended ship. Ship motions can be computed using a time stepping procedure using the following derived from Equation (30):

$$\begin{aligned}([M] \; + \; [A(U,\infty)]) \; \{\ddot{\eta}(t)\} \;\; = \;\; & - \; [b(U)] \; \left\{\dot{\eta(t)}\right\} \\ & - \; \int_{-\infty}^{t} [K(U,t-\tau)] \, \{\dot{\eta}(\tau)\} \; d\tau \\ & - \; ([C] \; + \; [c(U)]) \; \{\eta(t)\} \\ & + \; \left\{F^I(t) \; + \; F^D(t)\right\} \end{aligned} \tag{92}$$

The above system of equations enables computations of accelerations $\{\ddot{\eta}(t)\}$ provided that displacements and velocities are know up to time t. Hornbeck [17] discusses several numerical methods that can be used for integration of ship motions in the time domain. When selecting a suitable method, it is desirable to minimize the number of time steps at which forces need to be evaluated because of computational requirements. Another consideration is that when integrating displacements, both first and second derivatives (velocity and acceleration) are available. It was decided to use Taylor series for time-stepping of displacements and velocities. The Taylor series equations include contributions due to the time derivatives of accelerations, which are estimated using a backward difference approach. The following equations are evaluated in order to obtain displacements and velocities at time $t + \Delta t$ based on motions evaluated up to time t:

$$\frac{\partial \ddot{\eta}_j(t)}{\partial t} \;\; = \;\; \frac{23 \; \ddot{\eta}_j(t) \; - \; 16 \; \ddot{\eta}_j(t \; - \; \Delta t) + \; 5 \; \ddot{\eta}_j(t \; - \; 2\Delta t)}{12 \; t} \tag{93}$$

$$\eta_j(t \; + \Delta t) \;\; = \;\; \eta_j(t) \; + \; \Delta t \; \dot{\eta}_j(t) \; + \; \frac{(\Delta t)^2}{2} \; \ddot{\eta}_j(t) \; + \; \frac{(\Delta t)^3}{6} \; \frac{\partial \ddot{\eta}_j(t)}{\partial t} \tag{94}$$

$$\dot{\eta}_j(t \; + \Delta t) \;\; = \;\; \dot{\eta}_j(t) \; + \; \Delta t \; \ddot{\eta}_j(t) \; + \; \frac{(\Delta t)^2}{2} \; \frac{\partial \ddot{\eta}_j(t)}{\partial t} \tag{95}$$

When originally implementing the above equations into the Python computer code, arbitrary time step sizes Δt were facilitated using linear interpolation of results from previous time steps. Subsequent profiling of code execution revealed that a large amount of CPU was being devoted to interpolation of the retardation functions in Equation (92). To improve code efficiency, the code was re-written to restrict time step size to a single value input at the beginning of a simulation. This scheme gives much greater efficiency because retardation functions only need to be interpolated at the very beginning of a simulation using the input time step size. This coding change has increased execution speed by a factor of approximately 30 for linear time domain computations.

9 Comparison of Motions in the Time and Frequency Domains

To verify hydrodynamic coefficients and derived motions predicted in the time domain, comparisons have been made with frequency domain motion predictions. The predictions are for the HALIFAX using the medium mesh, with 433 panels on the port side of the hull. To give realistic roll motions, supplementary roll damping of 2×10^7 Nm/(rad/s) has been used, which is representative of damping from appendages and viscous effects. Similarly, supplementary yaw stiffness of 2×10^9 Nm/rad has been used, which is representative of the contributions of the skeg and rudder to coursekeeping stability.

A ship speed of 20 knots was selected for comparing frequency and time domain predictions. This speed was considered sufficiently high to verify consistency of speed dependent terms. The time domain computations are based on a time step size of 0.1 s, which gives excellent numerical stability. On a PC computer with a 800 MHz Pentium III processor, the time domain computations run approximately 30 times faster than real time. Figures 31 and 32 show excellent agreement between predictions in the frequency and time domains for both stern quartering and bow quartering seas. Note that the present theoretical approach deteriorates at very low encounter frequencies; thus, the predictions are limited to conditions with encounter frequencies $\geq$ 0.1 rad/s. This limitation can be handled from a practical standpoint by slightly shifting wave frequencies when travelling with forward speed in waves aft of the beam.

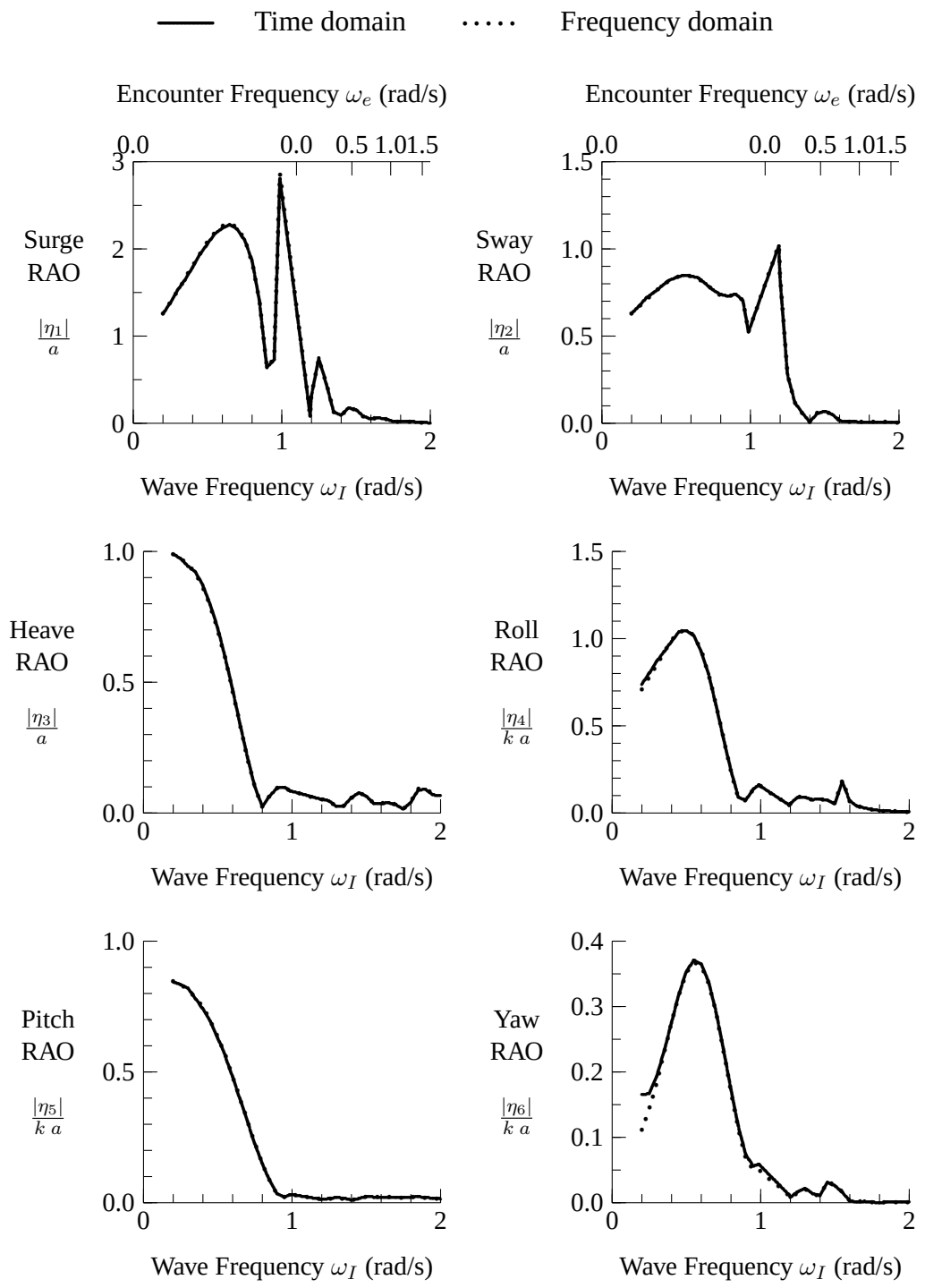

Figure 31: *Motions for HALIFAX from Frequency Domain and Time Domain Computations, Medium Mesh, 20 knots, Stern Quartering Seas at 30 degrees*

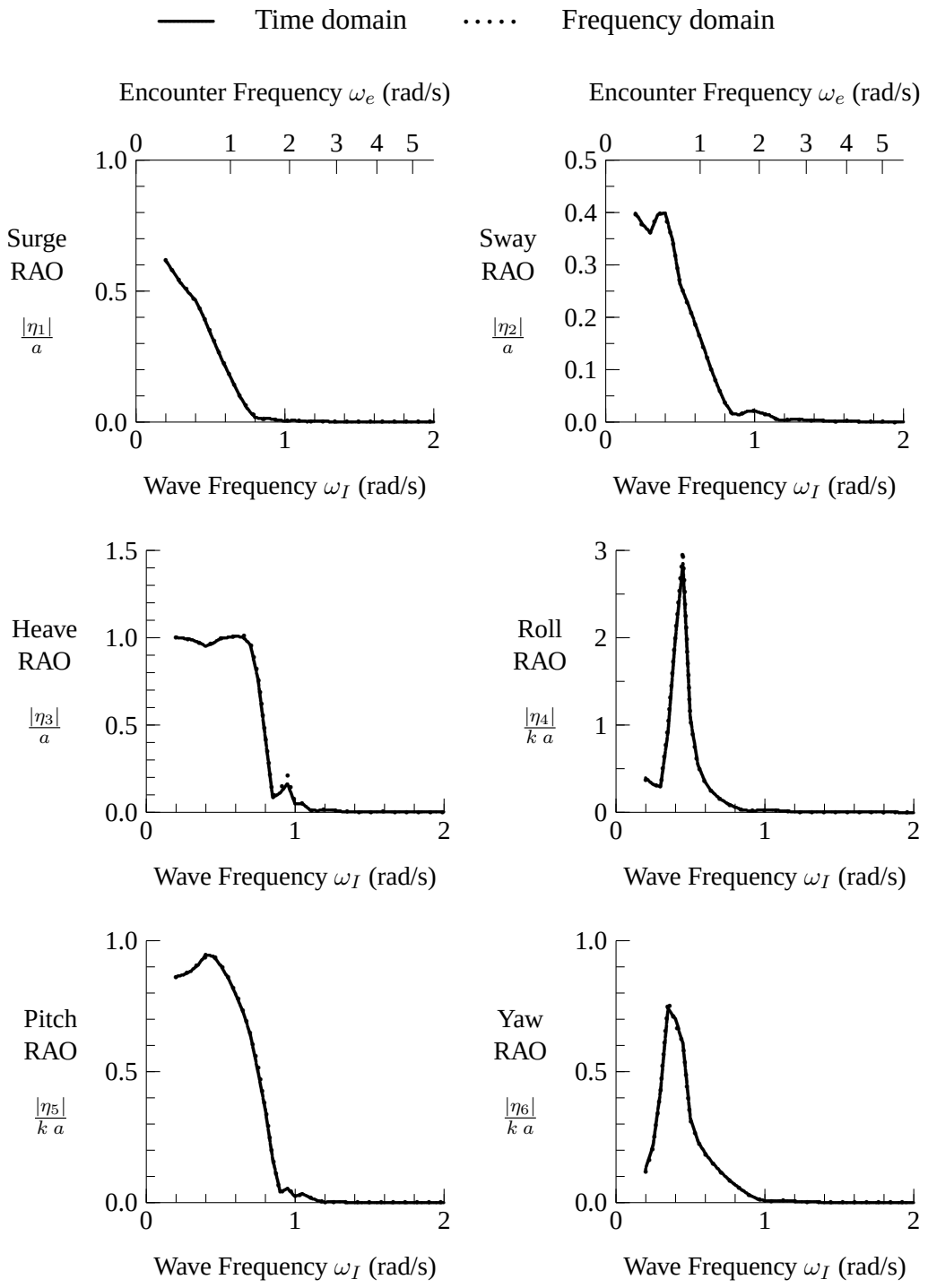

Figure 32: *Motions for HALIFAX from Frequency Domain and Time Domain Computations, Medium Mesh, 20 knots, Bow Quartering Seas at 150 degrees*

10 Extension to Nonlinear Forces from Incident Waves and Buoyancy

Time domain predictions presented thus far are based on linearized forces. It is relatively simple to extend the work to include nonlinear evaluation of forces due to incident waves and buoyancy. Furthermore, these two force components have large force magnitudes relative to other components such as radiation forces.

For evaluation of nonlinear forces, it is necessary to introduce a new ship-based coordinate system x^S, y^S, z^S that rotates with the ship, as shown in Figure 33 The origin of this coordinate system is at the ship centre of gravity. When wave-induced ship motions are zero, the ship-based coordinate system is identical to the coordinate system x, y, z based on translating earth axes presented in Figure 1.

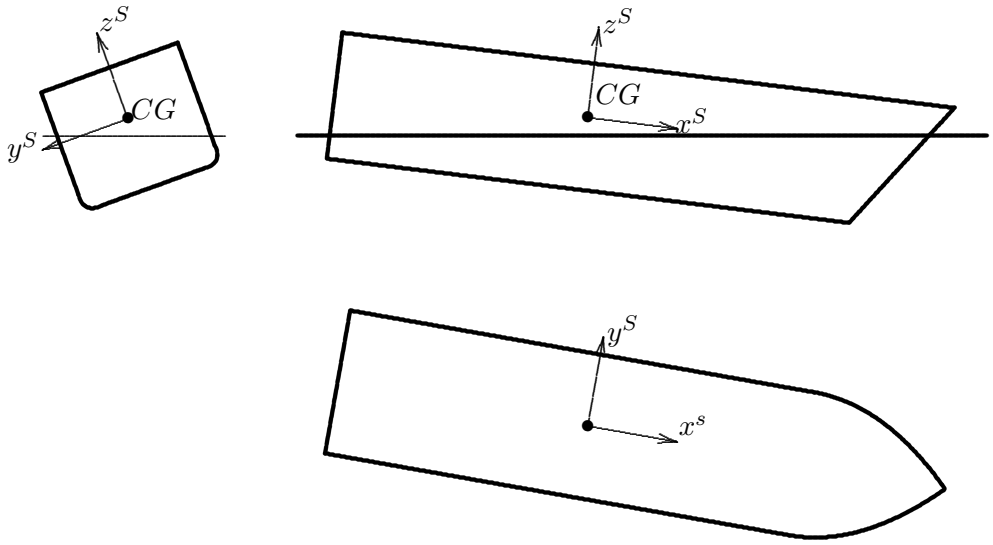

Figure 33: *Ship Referenced Coordinate System for Large Angular Motions*

Force components in the ship-based coordinate system are easily evaluated as follows:

$$F_j^S(t) \;=\; -\int_{S_b} p(t)\; n_j^S \; dS \text{ for } j = 1 - 6 \tag{96}$$

where n_j^S is the outward normal component for mode j in the ship-based coordinate system. The following equation can be used to obtain force components in

translating earth axes from force components computed using ship-based axes:

$$
\begin{aligned}
F_1(t) &= F_1^S(t)\ \cos\eta_6\ \cos\eta_5\ -\ F_2^S(t)\ \sin\eta_6\ \cos\eta_5 +\ F_3^S(t)\ \sin\eta_5 && (97)\\
F_2(t) &= F_1^S(t)\ (\cos\eta_6\ \cos\eta_5\ \sin\eta_4\ +\sin\eta_6\ \cos\eta_4)\\
&\quad + F_2^S(t)\ (-\sin\eta_6\ \sin\eta_5\ \sin\eta_4\ +\cos\eta_6\ \cos\eta_4)\\
&\quad - F_3^S(t)\ \sin\eta_4\ \cos\eta_5 && (98)\\
F_3(t) &= F_1^S(t)\ (-\cos\eta_6\ \sin\eta_5\ \cos\eta_4\ +\sin\eta_6\ \sin\eta_4)\\
&\quad + F_2^S(t)\ (\sin\eta_6\ \sin\eta_5\ \cos\eta_4\ +\cos\eta_6\ \sin\eta_4)\\
&\quad + F_3^S(t)\ \cos\eta_4\ \cos\eta_5 && (99)
\end{aligned}
$$

The above equations are based on rotations in the order of roll, pitch, and yaw when going from the translating earth to ship-based coordinate systems. Similarly, the location of a point on the ship can be converted to a location in translating earth axes as follows:

$$
\begin{aligned}
x(t) &= \eta_1\ +x^S\ \cos\eta_6\ \cos\eta_5\ -\ y^S\ \sin\eta_6\ \cos\eta_5 +\ z^S\ \sin\eta_5 && (100)\\
y(t) &= \eta_2\ +x^S\ (\cos\eta_6\ \cos\eta_5\ \sin\eta_4\ +\sin\eta_6\ \cos\eta_4)\\
&\quad + y^S\ (-\sin\eta_6\ \sin\eta_5\ \sin\eta_4\ +\cos\eta_6\ \cos\eta_4)\\
&\quad - z^S\ \sin\eta_4\ \cos\eta_5 && (101)\\
z(t) &= \eta_3\ +\ x^S\ (-\cos\eta_6\ \sin\eta_5\ \cos\eta_4\ +\sin\eta_6\ \sin\eta_4)\\
&\quad + y^S\ (\sin\eta_6\ \sin\eta_5\ \cos\eta_4\ +\cos\eta_6\ \sin\eta_4)\\
&\quad + z^S(t)\ \cos\eta_4\ \cos\eta_5 && (102)\\
z_{wl}(t) &= z(t)\ +\ \tilde{z}_{wl}^{CG} && (103)
\end{aligned}
$$

Equations (102) and (103) are required for evaluating the location of points on the hull within the wave field. Recall that $\tilde{z}_{wl}^{CG}$ is the height of the ship centre of gravity above the water surface when the ship is at rest in calm water.

The incident wave elevation in the time domain is given by Equation (46). The wave potential and its derivatives in the time domain are given by:

$$
\begin{aligned}
\Phi_I &= \frac{g\ a}{\omega_I}\ \sin\left[k_I\ (x\cos\beta\ -\ y\sin\beta)\ -\ \omega_e\ t\ -\ \epsilon_I\right]\ \exp(k_I\ z_{wl}) && (104)\\
\frac{\partial\Phi_I}{\partial x} &= a\ \omega_I\ \cos\beta\ \cos\left[k_I\ (x\cos\beta\ -\ y\sin\beta)\ -\ \omega_e\ t\ -\ \epsilon_I\right]\\
&\quad \times\exp(k_I\ z_{wl}) && (105)\\
\frac{\partial\Phi_I}{\partial y} &= -a\ \omega_I\ \sin\beta\ \cos\left[k_I\ (x\cos\beta\ -\ y\sin\beta)\ -\ \omega_e\ t\ -\ \epsilon_I\right]\\
&\quad \times\exp(k_I\ z_{wl}) && (106)\\
\frac{\partial\Phi_I}{\partial z} &= a\ \omega_I\ \sin\left[k_I\ (x\cos\beta\ -\ y\sin\beta)\ -\ \omega_e\ t\ -\ \epsilon_I\right]\ \exp(k_I\ z_{wl}) && (107)
\end{aligned}
$$

$$\frac{\partial \Phi_I}{\partial t} = -\frac{g\ a}{\omega_I}\ \omega_e\ \cos\left[k_I\ (x\cos\beta\ -\ y\sin\beta)\ -\ \omega_e\ t\ -\ \epsilon_I\right] \times \exp(k_I\ z_{wl}) \tag{108}$$

Using the above terms, the combined pressure due to incident wave forces and buoyancy can be evaluated as follows:

$$p(t) = -\rho\left(\frac{\partial \Phi_I}{\partial t}\ -\ U\ \frac{\partial \Phi_I}{\partial x}\ +\ g\ z_{wl}\right) \text{ for } z_{wl} \leq \zeta \tag{109}$$

$$p(t) = 0 \text{ for } z_{wl} > \zeta \tag{110}$$

Figures 34 to 36 show results of computations for verifying nonlinear buoyancy force predictions. For small displacements, the nonlinear buoyancy predictions show close agreement with linear buoyancy forces. For large heave displacements, nonlinear buoyancy forces approach limiting values as the ship hull becomes completely submerged (negative heave) or emerged (positive heave). The nonlinear roll buoyancy moments behave as expected, with symmetry about zero roll angle and vanishing righting moment at large roll angles. The nonlinear pitch buoyancy moments behave in a manner similar to the heave forces, with slope magnitude reducing when portions of the hull become completely submerged or emerged.

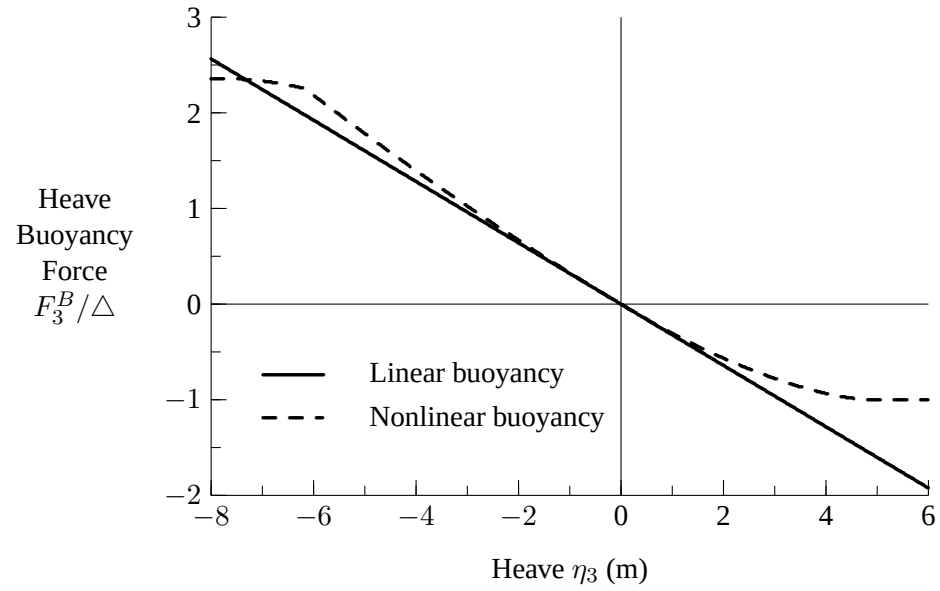

Figure 34: *Heave Buoyancy Forces for HALIFAX, Medium Mesh*

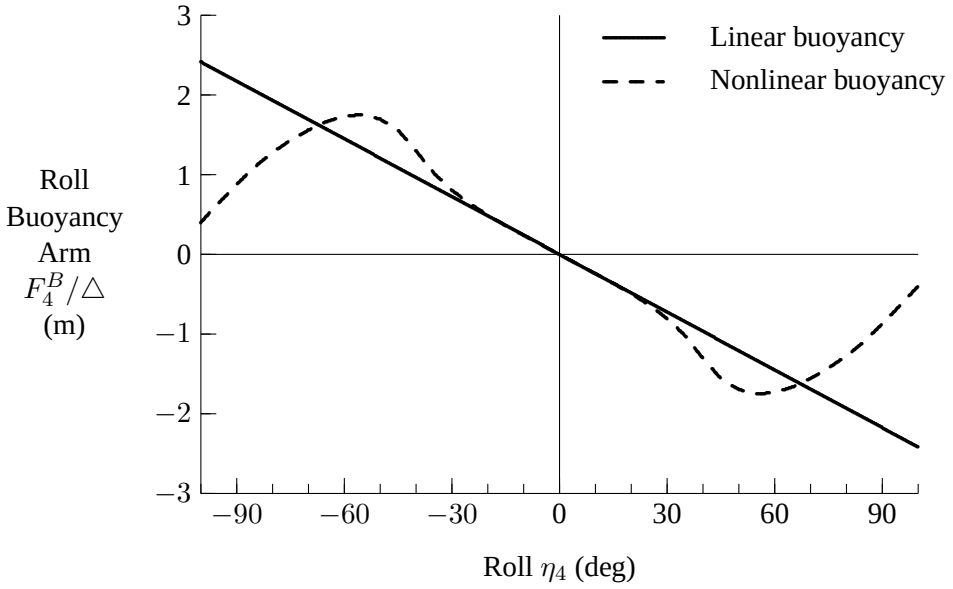

Figure 35: *Roll Buoyancy Moments for HALIFAX, Medium Mesh*

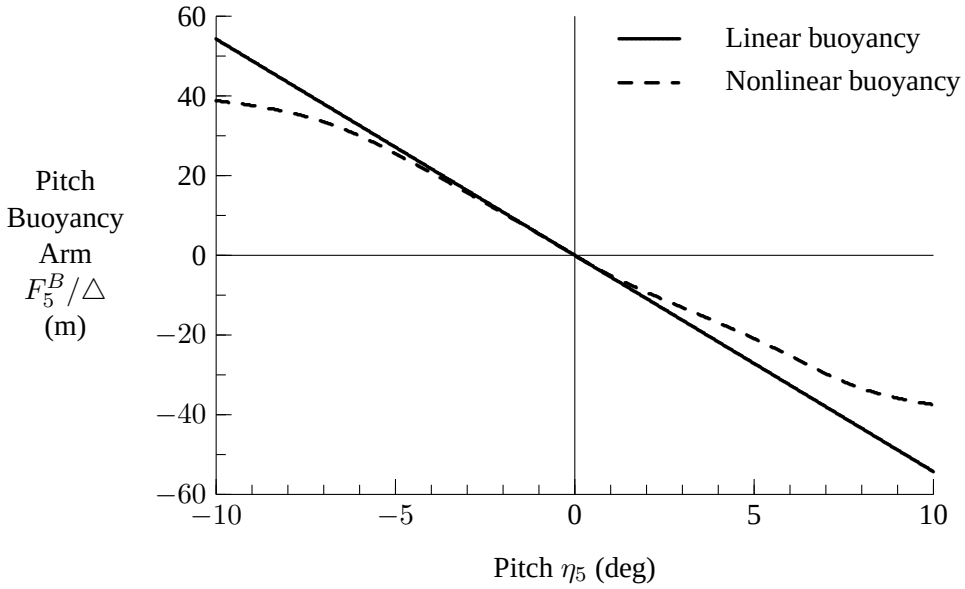

Figure 36: *Pitch Buoyancy Forces for HALIFAX, Medium Mesh*

11 Comparison of Numerical Predictions and Experimental Results for Heave and Pitch

The software testing presented thus far has been limited to verification, including comparison of predictions in the frequency and time domains. Validation of ship motion predictions generally requires comparison with measurements from model tests and/or sea trials. The current motion predictions do not include viscous or appendage forces, which can significantly influence lateral plane motions; however, predicted vertical plane predictions can be validated using experimental data.

Figures 37 and 38 show comparisons of heave and pitch predictions with experimental results for the CPF hydroelastic model in head seas [7]. The numerical predictions include the influence of restrained surge motions. The numerical predictions show very good agreement with experimental motions. As was observed in Section 9, frequency domain predictions correspond very closely to linear time domain predictions. The nonlinear predictions, which are for a wave steepness H/λ of 1/20, vary noticeably from the linear predictions. For the current heave and pitch cases, it appears that including nonlinear buoyancy and incident wave forces does not increase the accuracy of predictions. For intermediate wave frequencies at a Froude number of 0.20, Figure 38 suggests that including nonlinearities can actually give less accurate heave predictions. This observation could be due to modelling of larger amplitude waves using linear wave theory. To improve accuracy of nonlinear predictions in regular waves, a new regular wave model will be implemented using Stokes second order wave theory (see Sarpkaya and Isaacson [18]).

As mentioned in Section 9, the linear time domain simulations run approximately 30 times faster than real time when simulating a full-scale ship using a time step size of 0.1 s. When nonlinear buoyancy and incident wave forces are included using the medium mesh, computational speed is reduced to approximately 5 times faster than real time.

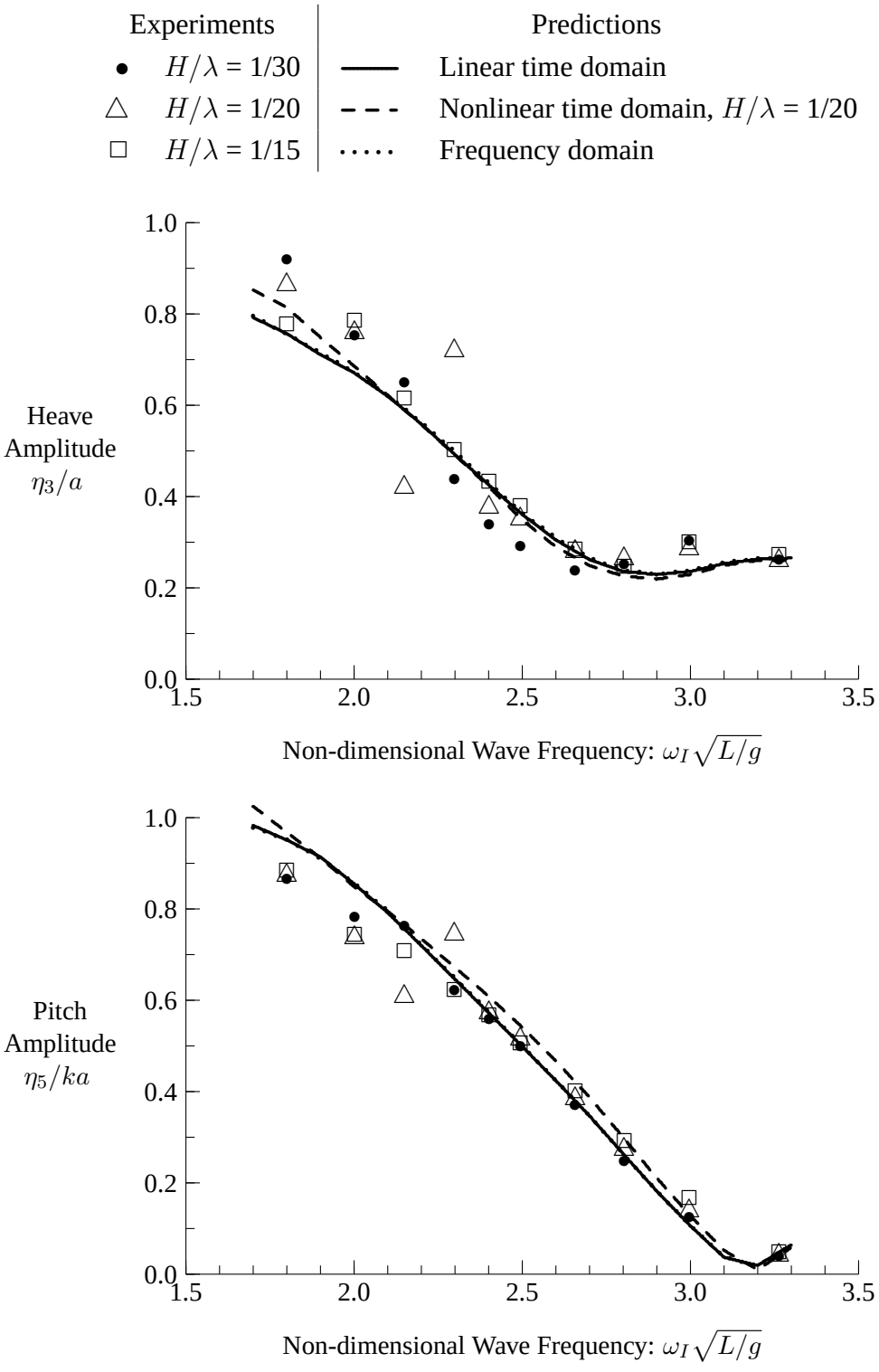

Figure 37: *Heave and Pitch for CPF Hydroelastic Model in Head Seas, Fn = 0.12*

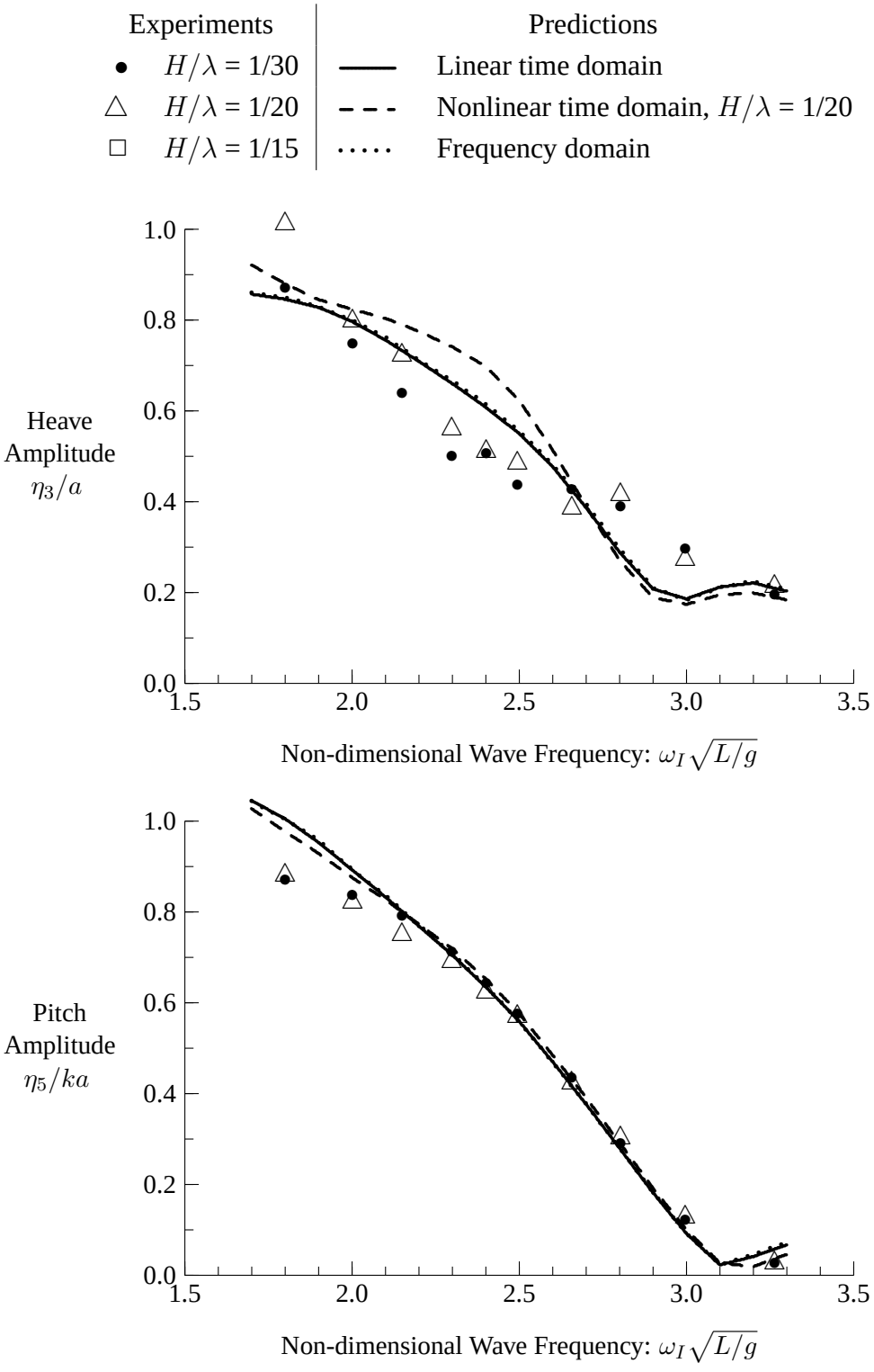

Figure 38: *Heave and Pitch for CPF Hydroelastic Model in Head Seas, Fn = 0.20*

12 Conclusions

New software has been developed for predicting hydrodynamic forces and resulting motions in the time domain for an unappended ship hull in waves. The ship is assumed to travel at steady speed and heading relative to the waves. The hydrodynamic forces in the time domain are evaluated using previously computed values in the frequency domain. Several improvements have been made to the accuracy, efficiency, and robustness of hydrodynamic force predictions in the frequency domain. Comparisons between predicted motions in the frequency and time domains indicate consistency between the two approaches. Initial validation using experimental motions for heave and pitch indicates that predictions in the frequency and time domains are giving good results. Nonlinear effects arising from incident wave and buoyancy forces can be included in time domain predictions.

In the near term, forces from rudders, bilge keels, and other appendages will be incorporated into numerical predictions of ship motions in waves. In the longer term, the motions of a freely maneuvering ship in waves will be predicted.

References

1. McTaggart, K.A. (2002). Three Dimensional Ship Hydrodynamic Coefficients Using the Zero Forward Speed Green Function. (DRDC Atlantic TM 2002-059). Defence Research and Development Canada - Atlantic.

2. Mei, C.C. (1983). The Applied Dynamics of Ocean Surface Waves, New York: John Wiley & Sons.

3. Wehausen, J.V. (1971). The Motion of Floating Bodies. *Annual Review of Fluid Mechanics,* **3**, 237–268.

4. McTaggart, K.A. (1989). Hydrodynamics and Risk Analysis of Iceberg Collisions with Offshore Structures. Ph.D. thesis. University of British Columbia.

5. Magee, A. (1994). Seakeeping Applications Using a Time Domain Method. In *Twentieth Symposium on Naval Hydrodynamics*, pp. 1–19. Santa Barbara.

6. Fonseca, N. and Soares, C. Guedes (1998). Time-Domain Analysis of Large-Amplitude Vertical Ship Motions and Wave Loads. *Journal of Ship Research,* **42**(2), 139–153.

7. McTaggart, K., Datta, I., Stirling, A., Gibson, S., and Glen, I. (1997). Motions and Loads of a Hydroelastic Frigate Model in Severe Seas. *Transactions, Society of Naval Architects and Marine Engineers*, Vol. 105.

8. Cook, R.D. (1981). Concepts and Applications of Finite Element Analysis, New York: John Wiley & Sons.

9. Sclavounos, P.D. and Lee, C. (1985). Topics on Boundary Element Solutions of Wave Radiation-Diffraction Problems. In *Fourth International Conference on Numerical Ship Hydrodynamics*, Washington.

10. Lutz, M. and Ascher, D. (1999). Learning Python, Sebastopol, CA: O'Reilly & Associates.

11. McTaggart, K.A. (1996). Improved Boundary Element Methods for Predicting Sectional Hydrodynamic Coefficients for Strip Theory Ship Motion Programs. (DREA TM 96/212). Defence Research Establishment Atlantic.

12. Ando, S. (2002). Lower Bounds to Irregular Frequencies in Wave-Ship Interactions for Engineering Applications. (DREA TM 2001-192). Defence Research Establishment Atlantic.

13. Lee, C.-H. and Sclavounos, P.D. (1989). Removing the Irregular Frequencies from Integral Equations in the Wave-Body Interactions. *Journal of Fluid Mechanics*, **207**, 393–418.

14. Hager, W.H. (1988). Applied Numerical Linear Algebra, Englewood Cliffs, New Jersey: Prentice-Hall.

15. Anderson, E., Bai, Z., Bischof, C., Demmel, J., Dongarra, J., Croz, J. Du, Greenbaum, A., Hammarling, S., McKenney, A., Ostrouchov, S., and Sorensen, D. (1995). LAPACK Users' Guide, Second ed. Philadelphia: Society for Industrial and Applied Mathematics.

16. Ascher, D., Dubois, P.F., Hinsen, K., Hugunin, J., and Oliphant, T. (2001). Numerical Python. (Technical Report UCRL-MA-128569). Lawrence Livermore National Laboratory. Livermore, California.

17. Hornbeck, R.W. (1975). Numerical Methods, New York: Quantum Publishers.

18. Sarpkaya, T. and Isaacson, M. (1981). Mechanics of Wave Forces on Offshore Structures, Van Nostrand Reinhold.

Symbols

$[A]$	added mass matrix
a	wave amplitude
B	ship beam
$[B]$	frequency domain damping matrix
$[b]$	dynamic damping matrix
$[C]$	hydrostatic stiffness matrix
$[c]$	dynamic stiffness matrix
CB	centre of buoyancy
$[D]$	normal flow velocity influence matrix
$even$	superscript denoting velocity potential is even function of y
$\left\{F^D\right\}$	diffracted wave force vector
$F_j^{D,U}$	diffracted force component proportional to U for mode j
F_j^{D,ω_e}	diffracted force component proportional to ω_e for mode j
$\left\{F^I\right\}$	incident wave force vector
F_j^S	force for mode j in ship-based coordinates
Fn	Froude number
FP	fore perpendicular
$\widetilde{G}_0$	frequency dependent term of Green function relative to zero frequency Green function
$\widetilde{G}_\infty$	frequency dependent term of Green function relative to infinite frequency Green function
g	gravitational acceleration
$[H]$	x velocity influence matrix
$[K]$	retardation function matrix
$[K^0]$	zero-speed component of retardation function matrix
$[K^U]$	component of retardation function matrix proportional to U
$[K^{UU}]$	component of retardation function matrix proportional to U^2
$\overline{KG}$	height of centre of gravity above baseline
k_I	incident wavenumber
L	ship length between perpendiculars
LCB	longitudinal centre of buoyancy
$[M]$	inertial matrix
n_k	outward normal component k for translating earth axes
n_k^S	outward normal component k for ship-based axes
N_p^{port}	number of panels on port side of hull
odd	superscript denoting velocity potential is odd function of y
p	pressure
$port$	superscript denoting port side of hull

R	distance from field point to source
R_1	distance from field point to source image
r_{xx}	roll radius of gyration
r_{yy}	pitch radius of gyration
r_{zz}	yaw radius of gyration
S_b	surface of floating body
S_k	surface of hull panel k
$star$	superscript denoting starboard side of hull
T_{mid}	draft at midships
t_s	trim by stern
U	ship speed
w_i	interpolation weight factor
x, y, z	translating earth axis coordinates
x^S, y^S, z^S	ship-based axis coordinates
$\vec{x}_s$	source location
$\tilde{z}_{wl}^{CG}$	height of ship centre of gravity above water surface in calm water
z_{wl}	z coordinate relative to calm water surface
β	wave direction relative to ship
Δt	time step size
δ_{jk}	Kroenecker delta function
ϵ_I	phase lead of incident wave
ζ_I	incident wave elevation
η_j	motion displacement in mode j
λ	matrix condition number
ρ	water density
$\{\sigma\}$	source strength vector
τ	delay time for convolution integral
Φ_I	incident wave potential in time domain
ϕ_D	diffracted wave potential in frequency domain
ϕ_I	incident wave potential in frequency domain
ϕ_k	radiated wave potential due to motion mode k
ϕ'_k	normalized potential for mode k at zero or infinite frequency limit
ω_I	incident wave frequency
ω_e	wave encounter frequency
ω_e^t	transition encounter frequency for Green function computation
$\triangle$	ship mass displacement

This page intentionally left blank.

DOCUMENT CONTROL DATA

(Security classification of title, body of abstract and indexing annotation must be entered when document is classified)

1. ORIGINATOR (the name and address of the organization preparing the document).
Defence R&D Canada - Atlantic

2. SECURITY CLASSIFICATION (overall security classification of the document including special warning terms if applicable)
UNCLASSIFIED

3. TITLE (The complete document title as indicated on the title page. Its classification should be indicated by the appropriate abbreviation (S,C,R or U) in parentheses after the title.)
Hydrodynamic Forces and Motions in the Time Domain for an Unappended Ship Hull

4. AUTHORS (Last name, first name, middle initial. If military, show rank, e.g. Doe, Maj. John E.)
McTaggart, Kevin A.

5. DATE OF PUBLICATION (month and year of publication of document)	6a. NO. OF PAGES (total including Annexes, Appendices, etc).	6b. NO. OF REFS (total cited in document)
May 2003	84	18

7. DESCRIPTIVE NOTES (The category of the document, e.g. technical report, technical note or memorandum. If appropriate, enter the type of report, e.g. interim, progress, summary, annual or final.)
Technical Memorandum

8. SPONSORING ACTIVITY (the name of the department project office or laboratory sponsoring the research and development. Include address).
Defence R&D Canada - Atlantic, PO Box 1012, Dartmouth, NS, Canada B2Y 3Z7

9a. PROJECT OR GRANT NO. (If appropriate, the applicable research and development project or grant number under which the document was written.)	9b. CONTRACT NO. (if appropriate, the applicable number under which the document was written).
11GK12	

10a. ORIGINATOR'S DOCUMENT NUMBER (the official document number by which the document is identified by the originating activity. This number must be unique.)	10b. OTHER DOCUMENT NOs. (Any other numbers which may be assigned this document either by the originator or by the sponsor.)
DRDC Atlantic TM 2003-104	

11. DOCUMENT AVAILABILITY (any limitations on further dissemination of the document, other than those imposed by security classification)

(X) Unlimited distribution
( ) Defence departments and defence contractors; further distribution only as approved
( ) Defence departments and Canadian defence contractors; further distribution only as approved
( ) Government departments and agencies; further distribution only as approved
( ) Defence departments; further distribution only as approved
( ) Other (please specify):

12. DOCUMENT ANNOUNCEMENT (any limitation to the bibliographic announcement of this document. This will normally correspond to the Document Availability (11). However, where further distribution (beyond the audience specified in (11) is possible, a wider announcement audience may be selected).

13. ABSTRACT (a brief and factual summary of the document. It may also appear elsewhere in the body of the document itself. It is highly desirable that the abstract of classified documents be unclassified. Each paragraph of the abstract shall begin with an indication of the security classification of the information in the paragraph (unless the document itself is unclassified) represented as (S), (C), (R), or (U). It is not necessary to include here abstracts in both official languages unless the text is bilingual).

This report describes numerical predictions of hydrodynamic forces and motions in the time domain for an unappended ship hull in waves. The hydrodynamic forces in the time domain are evaluated using previously computed values in the frequency domain, which are based on the three-dimensional Green function for a body with zero forward speed. Forward speed effects are included in both the frequency and time domains using suitable approximations. Due to the underlying importance of numerical predictions of hydrodynamic forces in the frequency domain, attention has been given to their accuracy, robustness, and efficiency. Comparisons between motion predictions in the frequency and time domains show excellent agreement, suggesting correct theoretical and numerical implementations. Comparisons of numerical heave and pitch predictions with model test data for the frigate HALIFAX show very good agreement. Time domain simulations of ship motion execute significantly faster than real time, indicating that the approach will be practical for modelling and simulation applications.

14. KEYWORDS, DESCRIPTORS or IDENTIFIERS (technically meaningful terms or short phrases that characterize a document and could be helpful in cataloguing the document. They should be selected so that no security classification is required. Identifiers, such as equipment model designation, trade name, military project code name, geographic location may also be included. If possible keywords should be selected from a published thesaurus. e.g. Thesaurus of Engineering and Scientific Terms (TEST) and that thesaurus-identified. If it not possible to select indexing terms which are Unclassified, the classification of each should be indicated as with the title).

heave
roll
pitch
seakeeping
ship motions
surge
time domain
sway
yaw

This page intentionally left blank.

Defence R&D Canada

Canada's leader in defence and national security R&D

R & D pour la défense Canada

Chef de file au Canada en R & D pour la défense et la sécurité nationale

www.drdc-rddc.gc.ca